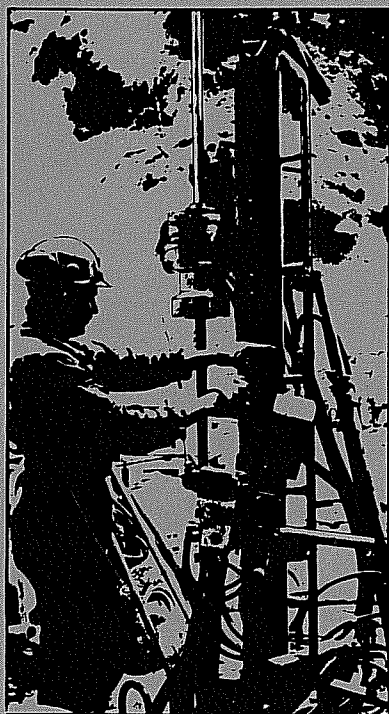


LBL-14929

SAC-41

UC-70

# SWEDISH-AMERICAN COOPERATIVE PROGRAM ON RADIOACTIVE WASTE STORAGE IN MINED CAVERNS IN CRYSTALLINE ROCK



Technical Information Report No. 41

## **PETROLOGIC CHANGES AND DAMAGE IN THE STRIPA QUARTZ MONZONITE IN RESPONSE TO HEATER TESTS**

S. Flexser, H. Wollenberg, and D. E. Wedge  
Lawrence Berkeley Laboratory  
University of California  
Berkeley, CA 94720

August 1982

A Joint Project of

Swedish Nuclear Fuel Supply Co.  
Fack 10240 Stockholm, Sweden

Operated for the Swedish  
Nuclear Power Utility Industry

Lawrence Berkeley Laboratory  
Earth Sciences Division  
University of California  
Berkeley, California 94720, USA

Operated for the U.S. Department of  
Energy under Contract DE-AC03-76SF00098

#### **LEGAL NOTICE**

This report was prepared as an account of work sponsored by the United States Government and/or the Swedish Nuclear Fuel Supply Company. Neither the United States nor the U.S. Department of Energy, nor the Swedish Nuclear Fuel Supply Company, nor any of their employees, nor any of their contractors, subcontractors, or their employees, makes any warranty, express or implied or assumes any legal liability or responsibility for the accuracy, completeness or usefulness of any information, apparatus, product or process disclosed, or represents that its use would not infringe privately owned rights.

Printed in the United States of America  
Available from  
National Technical Information Service  
U.S. Department of Commerce  
5285 Port Royal Road  
Springfield, VA 22161  
Price Code: A05

Lawrence Berkeley Laboratory is an equal opportunity employer.

LBL-14929  
SAC-41  
UC-70

PETROLOGIC CHANGES AND DAMAGE IN THE STRIPA QUARTZ  
MONZONITE IN RESPONSE TO HEATER TESTS

S. Flexser, H. Wollenberg, and D.E. Wedge

Earth Sciences Division  
Lawrence Berkeley Laboratory  
University of California  
Berkeley, California 94720

August, 1982

This work was supported by the Assistant Secretary for Nuclear Energy, Office of Waste Isolation, U.S. Department of Energy under contract DE-AC03-76SF00098. Funding for this project was administered by the Office of Nuclear Waste Isolation at Battelle Memorial Institute.



PREFACE

This report is one of a series documenting the results of the Swedish-American cooperative research program in which the cooperating scientists explore the geological, geophysical, hydrological, geochemical, and structural effects anticipated from the use of a large crystalline rock mass as a geologic repository for nuclear waste. This program has been sponsored by the Swedish Nuclear Power Utilities through the Swedish Nuclear Fuel Supply Company (SKBF), and the U.S. Department of Energy (DOE) through the Lawrence Berkeley Laboratory.

The principal investigators are L.B. Nilsson and O. Degerman for SKBF, and N.G.W. Cook, P.A. Witherspoon, and J.E. Gale for LBL. Other participants will appear as authors of the individual reports.

Previous technical reports in this series are listed below.

1. Swedish-American Cooperative Program on Radioactive Waste Storage in Mined Caverns by P.A. Witherspoon and O. Degerman. (LBL-7049, SAC-01).
2. Large Scale Permeability Test of the Granite in the Stripa Mine and Thermal Conductivity Test by Lars Lundstrom and Haken Stille. (LBL-7052, SAC-02).
3. The Mechanical Properties of the Stripa Granite by Graham Swan. (LBL-7074, SAC-03).
4. Stress Measurements in the Stripa Granite by Hans Carlsson. (LBL-7078, SAC-04).
5. Borehole Drilling and Related Activities at the Stripa Mine by P.J. Kurfurst, T. Hugo-Persson, and G. Rudolph. (LBL-7080, SAC-05).
6. A Pilot Heater Test in the Stripa Granite by Hans Carlsson. (LBL-7086, SAC-06).
7. An Analysis of Measured Values for the State of Stress in the Earth's Crust by Dennis B. Jamison and Neville G.W. Cook. (LBL-7071, SAC-07).
8. Mining Methods Used in the Underground Tunnels and Test Rooms at Stripa by B. Andersson and P.A. Halen. (LBL-7081, SAC-08).
9. Theoretical Temperature Fields for the Stripa Heater Project by T. Chan, Neville G.W. Cook, and C.F. Tsang. (LBL-7082, SAC-09).
10. Mechanical and Thermal Design Considerations for Radioactive Waste Repositories in Hard Rock. Part I: An Appraisal of Hard Rock for Potential Underground Repositories of Radioactive Waste by N.G.W. Cook; Part II: In Situ Heating Experiments in Hard Rock: Their Objectives and Design by N.G.W. Cook and P.A. Witherspoon. (LBL-7073, SAC-10).
11. Full-Scale and Time-Scale Heating Experiments at Stripa: Preliminary Results by N.G.W. Cook and M. Hood. (LBL-7072, SAC-11).
12. Geochemistry and Isotope Hydrology of Groundwaters in the Stripa Granite: Results and Preliminary Interpretation by P. Fritz, J.F. Barker, and J.E. Gale. (LBL-8285, SAC-12).
13. Electrical Heaters for Thermo-Mechanical Tests at the Stripa Mine by R.H. Burleigh, E.P. Binnall, A.O. DuBois, D.O. Norgren, and A.R. Ortiz. (LBL-7063, SAC-13).
14. Data Acquisition, Handling, and Display for the Heater Experiments at Stripa by Maurice B. McEvoy. (LBL-7063, SAC-14).
15. An Approach to the Fracture Hydrology at Stripa: Preliminary Results by J.E. Gale and P.A. Witherspoon. (LBL-7079, SAC-15).
16. Preliminary Report on Geophysical and Mechanical Borehole Measurements at Stripa by P. Nelson, B. Paulsson, R. Rachiele, L. Andersson, T. Schrauf, W. Hustrulid, O. Duran, and K.A. Magnussen. (LBL-8280, SAC-16).
17. Observations of a Potential Size-Effect in Experimental Determination of the Hydraulic Properties of Fractures by P.A. Witherspoon, C.H. Amick, J.E. Gale, and K. Iwai. (LBL-8571, SAC-17).
18. Rock Mass Characterization for Storage in Nuclear Waste in Granite by P.A. Witherspoon, P. Nelson, T. Doe, R. Thorpe, B. Paulsson, J.E. Gale, and C. Forster. (LBL-8570, SAC-18).
19. Fracture Detection in Crystalline Rock Using Ultrasonic Shear Waves by K.H. Waters, S.P. Palmer, and W.F. Farrell. (LBL-7051, SAC-19).

20. Characterization of Discontinuities in the Stripa Granite--Time Scale Heater Experiment by R. Thorpe. (LBL-7083, SAC-20).
21. Geology and Fracture System at Stripa by A. Okliewicz, J.E. Gale, R. Thorpe, and B. Paulsson. (LBL-8907, SAC-21).
22. Calculated Thermally Induced Displacements and Stresses for Heater Experiments at Stripa by T. Chan and N.G.W. Cook. (LBL-7061, SAC-22).
23. Validity of Cubic Law for Fluid Flow in a Deformable Rock Fracture by P.A. Witherspoon, J. Wang, K. Iwai, and J.E. Gale. (LBL-9557, SAC-23).
24. Determination of In-Situ Thermal Properties of Stripa Granite from Temperature Measurements in the Full-Scale Heater Experiments: Methods and Primary Results by J. Jeffry, T. Chan, N.G.W. Cook and P.A. Witherspoon. (LBL-8424, SAC-24).
25. Instrumentation Evaluation, Calibration, and Installation for Heater Tests Simulating Nuclear Waste in Crystalline Rock, Sweden by T. Schrauf, H. Pratt, E. Simonson, W. Hustrulid, P. Nelson, A. DuBois, E. Binnall, and R. Haught. (LBL-8313, SAC-25)
26. Part I: Some Results From a Field Investigation of Thermo-Mechanical Loading of a Rock Mass When Heater Canisters are Emplaced in the Rock by M. Hood. Part II: The Application of Field Data from Heater Experiments Conducted at Stripa, Sweden for Repository Design by M. Hood, H. Carlsson, and P.H. Nelson. (LBL-9392, SAC-26).
27. Progress with Field Investigations at Stripa by P.A. Witherspoon, N.G.W. Cook, and J.E. Gale (LBL-10559, SAC-27).
28. A Laboratory Assessment of the Use of Borehole Pressure Transients to Measure the Permeability of Fractured Rock Masses by C.B. Forster and J.E. Gale. (LBL-8674, SAC-28).
29. Thermal and Thermomechanical Data for In Situ Heater Experiments at Stripa, Sweden by T. Chan, E. Binnall, P. Nelson, O. Wan, C. Weaver, K. Ang, J. Braley, and M. McEvoy. (LBL-11477, SAC-29).
30. The Effect of Radon Transport in Groundwater Upon Gamma Ray Borehole Logs by P.H. Nelson, R. Rachiele, and A. Smith. (LBL-11180, SAC-30).
31. Strength and Permeability Tests on Ultra-Large Stripa Granite Core by R. Thorpe, D.J. Watkins, W.E. Ralph, R. Hsu, and S. Flexser. (LBL-11203, SAC-31).
32. Ultrasonic and Acoustic Emission Results from the Stripa Heater Experiments. Part I: A Cross-Hole Investigation of a Rock Mass Subjected to Heating by B.N.P. Paulsson and M.S. King. Part II: Acoustic Emission Monitoring During Cool-Down of the Stripa Heater Experiment by R. Rachiele. (LBL-10975, SAC-32).
33. Numerical Modeling to Assess Possible Influence of the Mine Openings on Far-Field In Situ Stress Measurements at Stripa by T. Chan, V. Guvanasen, and N. Littlestone (LBL-12469, SAC-33).
34. A Field Assessment of the Use of Borehole Pressure Transients to Measure the Permeability of Fractured Rock Masses by C.B. Forster and J.E. Gale. (LBL-11829, SAC-34).
35. Water Inflow into Boreholes During the Stripa Experiments by P.H. Nelson, R. Rachiele, J.S. Remer and H.S. Carlsson (LBL-12547, SAC-35).
36. Petrology and Radiogeology of the Stripa Pluton by H. Wollenberg, S. Flexser, and L. Andersson. (LBL-11654, SAC-36).
37. Geohydrological Data from the Macopermeability Experiment at Stripa, Sweden by C.R. Wilson, J.C.S. Long, R.M. Galbraith, K. Karasaki, H.K. Endo, A.O. DuBois, M.J. McPherson, and G. Ramqvist. (LBL-12520, SAC-37).
38. Characterization of Discontinuities in the Stripa Granite--Full-Scale Heater Experiments by B.N.P. Paulsson, P.H. Nelson, and P.J. Kurfurst. (LBL-9063, SAC-38).
39. Application of Borehole Geophysics at an Experimental Waste Storage Site by P.H. Nelson, K.A. Magnusson, and R. Rachiele. (LBL-11982, SAC-39).
40. Laboratory Investigations of Thermomechanical Properties of Stripa Granite by L. Myer and R. Rachiele. (LBL-13435, SAC-40)

TABLE OF CONTENTS

	<u>Page</u>
LIST OF FIGURES . . . . .	vii
LIST OF TABLES . . . . .	ix
ABSTRACT . . . . .	xi
1. INTRODUCTION . . . . .	1
2. PETROLOGIC EXAMINATIONS. . . . .	7
2.1 Thin Section Petrography. . . . .	7
2.1.1 Mineralogic Alterations. . . . .	9
2.1.2 Microfracturing. . . . .	12
2.2 X-Ray Diffraction Analyses. . . . .	13
2.2.1 Description of Samples and Sample Preparation. . . . .	13
2.2.2 Diffraction Analyses of Chlorite from the Drillback Cores. . . . .	14
2.2.2.1 Powder Pattern Analyses . . . . .	14
2.2.2.2 Single Crystal Analyses . . . . .	18
2.2.3 Diffraction Analyses of Chlorite Samples from Quartz Monzonite Heated in the Laboratory . . . . .	20
2.2.4 Diffraction Analyses of Muscovite. . . . .	24
2.3 Electron Microprobe Analyses. . . . .	26
2.3.1 Chlorite . . . . .	26
2.3.2 Muscovite. . . . .	33
2.4 Alpha-Radiographic and Gamma-Spectrometric Analyses . . . . .	39
2.4.1 Alpha Radiography. . . . .	40
2.4.2 Gamma Spectrometry . . . . .	49
3. BOREHOLE STEREOPHOTOGRAPHY . . . . .	55
4. SUMMARY AND CONCLUSIONS. . . . .	61
ACKNOWLEDGMENTS. . . . .	67
REFERENCES . . . . .	69



LIST OF FIGURES

	<u>Page</u>
1. Locations of full-scale heaters, peripheral heaters, and extensometers in vertical and horizontal boreholes, Stripa mine experimental area (from Witherspoon et al., 1980) . . . . .	2
2. (A) Measured temperatures following turn-on of the peripheral heaters, at varying distances from the H-10 heater hole along heater midplane (from Javandel and Witherspoon, 1981). (B) Projected temperature fields in rock surrounding the H-10 heater array along heater midplane (from Chan et al., 1980). . . . .	3
3. Vertical cross-section through the H-10 heater hole and the heater and extensometer drifts, showing the location of drillback holes. . . . .	5
4. Variation of U, Th, and K with distance from the H-10 heater and comparison with analyses of unheated Stripa rock . . . . .	52
5. (A) Plan of H-10 heater hole, showing positions of the four vertical transects corresponding to the profiles in Fig. 6. Camera position is along transect 2. (B) Cross-section of H-10 heater hole, showing camera positioned as in (A) and scale located opposite camera . . . . .	56
6. Decrepitation profiles from the H-10 heater hole, located along the positions of the vertical transects shown in Fig. 5A . . . . .	57



LIST OF TABLES

	<u>Page</u>
1. Diffraction patterns of chlorite separates. . . . .	15
2. Estimated errors in reading of diffraction lines. . . . .	16
3. Diffraction pattern of magnetic fraction from sample of quartz monzonite heated in laboratory . . . . .	22
4. Diffraction patterns of muscovite separates . . . . .	25
5. Mean chlorite analyses by electron microprobe . . . . .	27
6. Mean ionic abundances and structural formulas of chlorites analyzed by microprobe. . . . .	31
7. Mean muscovite analyses by electron microprobe. . . . .	34
8. Mean ionic abundances and structural formulas of muscovites analyzed by microprobe. . . . .	37
9. Uranium-thorium concentrations in typical sites in heated and unheated quartz monzonite . . . . .	46
10. Analyses of heated and unheated quartz monzonite samples by gamma spectrometry . . . . .	51



ABSTRACT

The effects of underground in situ heating of quartz monzonite at Stripa, Sweden, were studied with respect to petrologic alterations and mechanical damage to the rock. A suite of core samples obtained from holes drilled through the walls of the H-10 heater hole was examined in thin sections, by x-ray diffraction, and by electron microprobe. Mineralogic alterations in the rock adjacent to the heater were most pronounced for chlorite, which showed a marked change in color associated with proximity to fractures as well as to the heater hole. Structural changes in chlorite included decrease in the dimensions of the unit cell, a change to hexagonal or pseudo-hexagonal symmetry, and possibly disorder in layer stacking perpendicular to the c-axis. Intergrowth of fine hematite with chlorite also occurred. Chemically, chlorite from near the heater was relatively consistent in composition over varying distances from the heater hole, but fracture-filling chlorite and chlorite in the rock matrix showed differences in composition. Overall, chlorite from near the heater differed from chlorite in unheated Stripa rock mainly with respect to  $\text{SiO}_2$ ,  $\text{MgO}$ , and  $\text{FeO}$ . Muscovite in the in situ-heated rock showed faint color changes associated with heating but was structurally unaltered. Muscovite near the heater hole was generally consistent in chemical composition, although it showed some variability at grain margins and in fracture fillings.

A specimen of Stripa quartz monzonite heated to  $600^\circ\text{C}$  in the laboratory was studied for comparison with the in situ-heated rock. Chlorite in this specimen was largely recrystallized to an intergrowth of hematite and other iron oxides and hydroxides, which also differed from chlorite in the in situ-heated rock in its abundances of  $\text{H}_2\text{O}$ ,  $\text{MgO}$ , and  $\text{K}_2\text{O}$ . Muscovite in

this specimen differed markedly in its optical properties from muscovite in the in situ-heated rock; it also had larger unit cell dimensions and/or was intergrown with a mineral in the biotite-phlogopite series. Chemically, it differed from muscovite in the in situ-heated rock in its abundances of  $H_2O$ ,  $K_2O$ ,  $Na_2O$ , and  $Al_2O_3$ .

The distribution of uranium and thorium in the in situ-heated rock was studied by alpha radiography, which provided qualitative evidence for the addition of U or Th to sites of disseminated accumulations of these elements in samples near the heater hole. These accumulations occurred in fractures, cleavage planes, and grain boundaries. Sources of the added U or Th were not positively identified, but gamma-spectral analyses suggested depletion of these elements in rock away from the heater and their migration toward the heater hole.

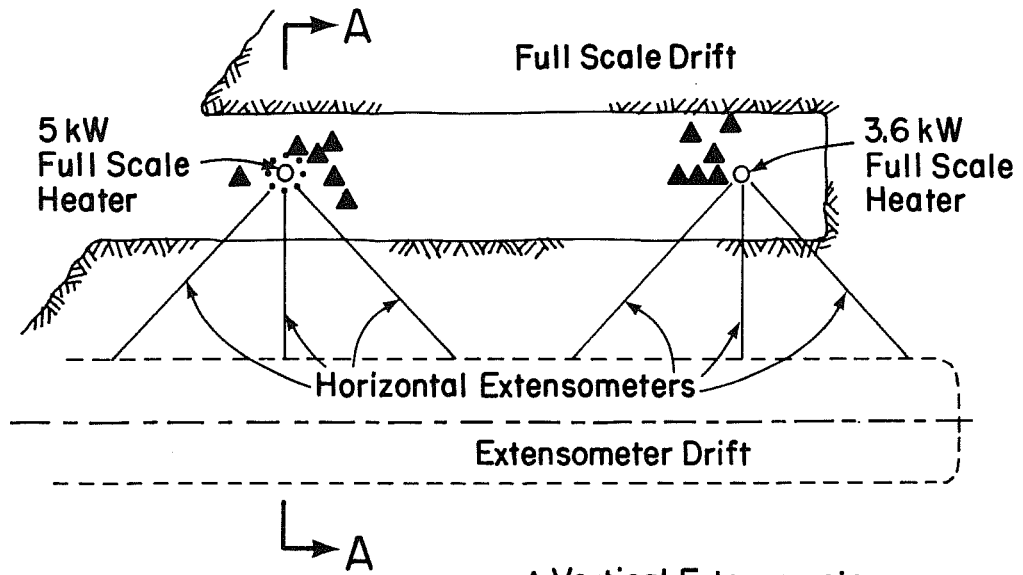
Mechanical damage to the rock surrounding the heater was assessed by stereophotographic surveys of the heater hole. Maximum depth of decrepitation observed was ~8 cm, and the depth averaged 1.7 cm over the length of the heater. Rock spalled from the heater hole contained fine fractures oriented tangentially to the hole. But the decrepitation had no apparent preferred orientation that could be attributed directly to stresses from the underground galleries or in the intact rock mass.

## 1. INTRODUCTION

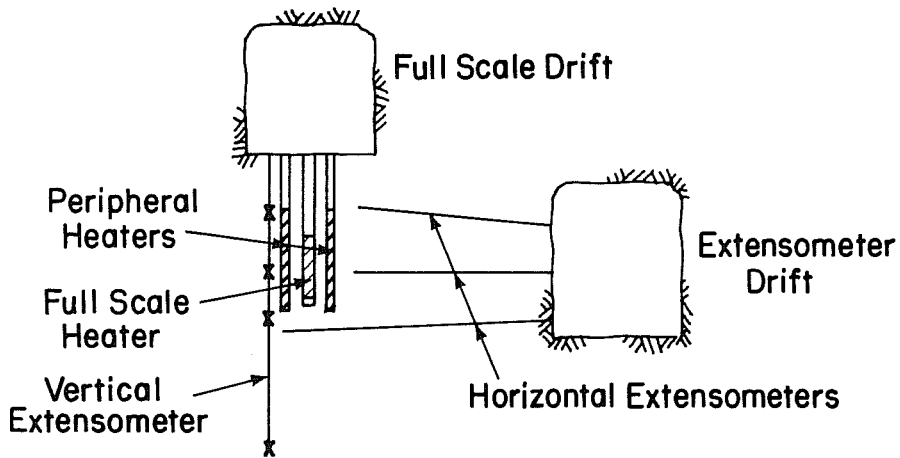
The heater experiment at Stripa was undertaken to determine the effects of prolonged in situ heating on fractured granitic rock and groundwater flow. This study assesses the petrologic effects on, and the mechanical damage to, the rock surrounding the H-10 heater, one of two main heaters employed in the experiment.

This 5-kW heater, a cylinder 0.3 m in diameter and 2.6 m long, was emplaced in a vertical hole 0.4 m in diameter drilled in the floor of the full-scale drift at the 340-m level of the Stripa mine. Surrounding the H-10 heater, at a radius of 0.9 m from its axis, was a ring of eight peripheral 1-kW heaters, centered on the same horizontal plane as the central heater (Witherspoon et al., 1980). Figure 1 illustrates, in plan view and in cross-section, the geometry of these heaters in relation to the full-scale and extensometer drifts.

Figure 2 shows, as a function of time, the temperatures reached by the rock surrounding the central heater, H-10, at its horizontal midplane. After H-10 had been running at 5 kW full power for 200 days, the peripheral heaters were switched on, and both central and peripheral heaters continued running another 200 days. The peripheral heaters were kept at full power (1 kW) for 40 days, then lowered to 0.85 kW for the remaining 160 days. Figure 2(B) shows the projected temperature fields in surrounding rock at radial distances up to 4 m from the central heater, and Fig. 2(A) shows the measured temperatures, following turn-on of the peripheral heaters, in rock at radial distances of between 0.2 m and 0.7 m from the edge of the H-10 heater hole.



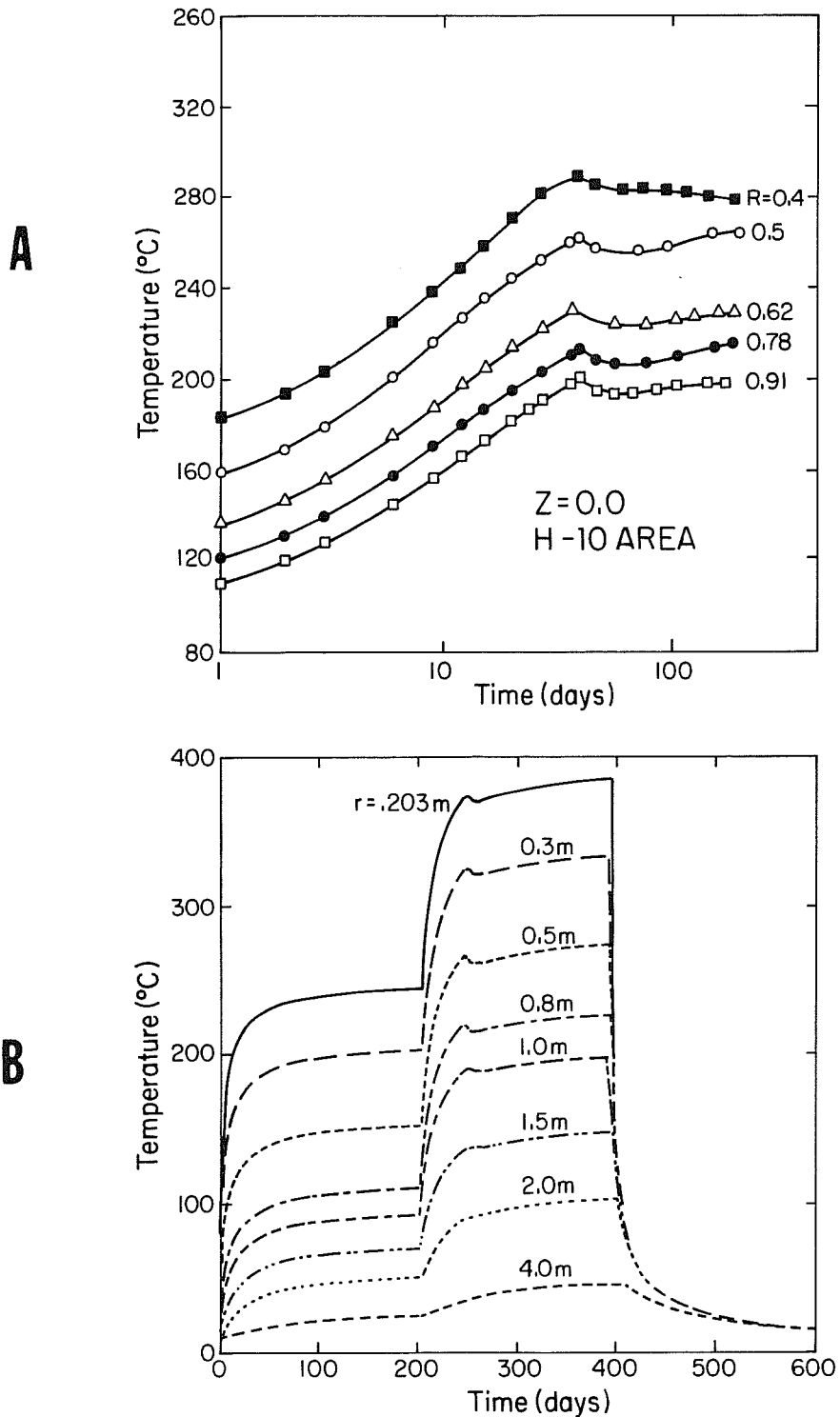
△ Vertical Extensometers  
• Peripheral Heaters



A - A

XBL 801 - 4588

Fig. 1. Locations of full-scale heater heaters, peripheral heaters, and extensometers in vertical and horizontal boreholes, Stripa mine experimental area (from Witherspoon et al., 1980).

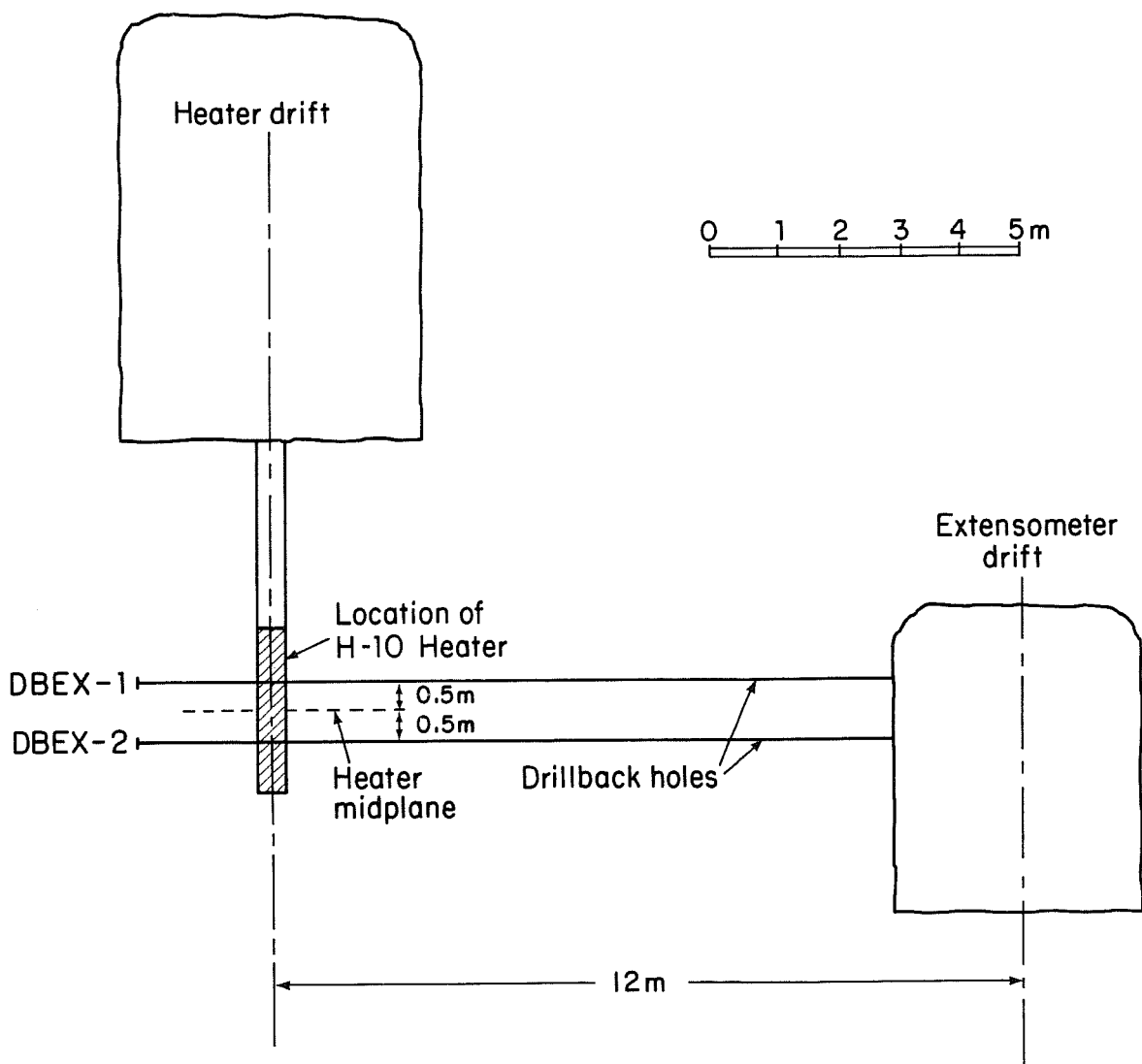


XBL 829-2389

Fig. 2. (A) Measured temperatures following turn-on of the peripheral heaters, at varying distances from the H-10 heater hole along heater midplane (from Javandel and Witherspoon, 1981). (B) Projected temperature fields in rock surrounding the H-10 heater array along heater midplane (from Chan et al., 1980).

In the course of the heater tests, decrepitation of the walls of the heater holes was observed. Spalling occurred and increased significantly after the peripheral heaters were turned on (Hood et al., 1979). To assess the extent of this damage, a detailed stereophotographic survey of the heater holes was made after the heaters were shut down and removed and the rock had returned to ambient temperature. The results and preliminary interpretations of this survey are the subjects of Section 3.

Following the photographic surveys, two continuously-cored horizontal holes (henceforth referred to as the "drillback cores") were drilled from the extensometer drift, through and beyond the H-10 heater hole; these holes were spaced vertically 0.5 m above and below the midplane of the H-10 heater (Fig. 3). Sections of the drillback cores were subjected to petrographic, x-ray diffraction, electron microprobe, alpha-autoradiographic, and gamma-spectrometric examinations. The results, the principal subject of this report, are described in Section 2.



XBL 829-2391

Fig. 3. Vertical cross-section through the H-10 heater hole and the heater and extensometer drifts, showing the location of drillback holes.



## 2. PETROLOGIC EXAMINATIONS

A major focus of this study concerned mineralogic alterations--particularly in the phyllosilicate minerals chlorite and muscovite--that occurred as a result of the heater experiment. These alterations were studied in thin section, in detailed x-ray diffraction analyses, and by electron microprobe. A second major focus concerned the possibility of migration and redistribution of the radioelements uranium and thorium in the drillback cores. This part of the study used alpha radiography of core sections in conjunction with whole-rock gamma spectrometry.

### 2.1 Thin Section Petrography

The drillback cores were obtained from two holes drilled from the extensometer drift (Fig. 3). The cores were composed entirely of Stripa quartz monzonite. Mineralogically, this quartz monzonite is predominantly a feldspar-quartz intergrowth, with roughly equal volumes of quartz, Na-rich plagioclase feldspar, and K-rich microcline feldspar which together comprise 90% or more of the rock (Wollenberg et al., 1980). The two other principal minerals of this rock are chlorite (formed in large part by alteration of primary biotite) and muscovite, together making up an additional 6-10%. The quartz monzonite is highly fractured and brecciated on both microscopic and macroscopic scales, and fracture-filling materials are most commonly chlorite, sericite, quartz, and epidote (Wollenberg et al., 1980).

In the drillback core from rock immediately adjacent to the heater hole, two changes in the quartz monzonite were apparent in hand specimen: chlorite in fractures and in isolated grain aggregates within 10 cm of the heater hole was changed from its normal dark green color to dark red-brown; and the rock was faintly but distinctly lighter and pinker in color within 20 cm of the hole.

To understand these alterations, to see whether others were visible microscopically, and to determine whether there was a progression in alteration with distance from the heater, thin sections from the drillback cores were cut at regular intervals away from the edge of the heater hole. (Because of decrepitation, the hole's diameter had increased from the original 41 cm by 5 and 11 cm where it was intersected by the drillback cores. Distances to sample locations were therefore adjusted to account for this change by adding half of the increase in diameter to the actual distance measured between the edge of the decrepitated wall and the end of the core). In one drill core, thin sections were cut from a surface parallel to the core axis and perpendicular to the heater axis, providing a continuous sampling in thin section of that surface to a distance of 50 cm from the edge of the heater hole. In the other core, thin sections were cut perpendicular to the core axis, at intervals of 1 to 3 cm, to a distance of 20 cm from the edge of the hole. Thin sections were also cut from pieces of spalled rock that were recovered from the floor of the hole.

For a qualitative comparison with these heater-adjacent samples, thin sections were also cut from a cylindrical block of Stripa quartz monzonite (12 cm diam, and 6 cm thick) that had been heated to 600°C in a laboratory oven over a period of 3 weeks (L. Andersson, personal communication). This sample, although heated under very different conditions of pressure and fracture fluid flow than the rock near the heaters, provided a qualitative comparison with that rock, and a chance to see whether the alterations resulting from this intensive heating would represent an advanced state of the alterations seen in the drillback cores.

### 2.1.1 Mineralogic Alterations

In thin section, the most pronounced alteration in the rock adjacent to the heater was the color change in chlorite. Muscovite grains also showed alteration not apparent megascopically, but this was much less striking than that of chlorite and was confined to grain edges. The faint color change in the quartz monzonite was not, however, observed readily in the microscope. Clouding of plagioclase grains could sometimes be seen in thin section, and was probably caused either by minute, submicroscopic clay alteration or by oxidation of iron impurities in the feldspar, or both. The megascopic color change of the rock, turning paler and pinker within about 20 cm from the edge of the heater hole, was therefore interpreted as a composite of these alterations of feldspar grains.

The mineralogic changes in chlorite and muscovite were the major heater-induced alterations of the quartz monzonite observable in thin section. Chlorite in Stripa quartz monzonite is common both as fine fracture-filling material, where it is usually intergrown with sericite, quartz, or epidote, and as coarser crystals, altered from the original biotite and intergrown with muscovite. In all these contexts, chlorite was thoroughly altered to a deep red-brown material in samples spalled from the wall of the heater hole, but it remained entirely green and unaltered beyond ~10 cm from the edge of the hole. Between these zones, a transitional type of chlorite was commonly observed, wherein grain edges were altered to form red-brown rinds enclosing green and unaltered cores. In this transitional zone, chlorite was preferentially altered near major fractures, while in the finest stringers ( $\leq 20 \mu\text{m}$  in width), or within quartz or feldspar grains, it was often green and unaltered. It thus seems likely that circulating water played an important role in the

alteration of chlorite, and that heating alone was insufficient. It should also be noted that coarse epidote-filled fractures, about 1-2 mm in width, seen in thin sections 8 cm from the heater hole, also had a marked orange coloration not observed in similar fractures in the unheated samples. The epidote grains themselves, however, did not appear to be altered. Instead, the coloration was confined to interstices between grains. This coloration was due to finely-disseminated hematite, to pigmentary coatings on the epidote grains, or to alteration of extremely fine interstitial chlorite.

Two morphological types of chlorite crystals can be distinguished in the quartz monzonite. The first and more common type consists of blocky crystals in knotlike aggregates or clusters intergrown with fine sericite or coarser muscovite, both in the rock matrix and in fractures. The second type consists of individual thin platelets or flakes usually interleaved with coarse muscovite grains along cleavage surfaces. These two types are not necessarily different mineralogically; the distinction is based simply on the different contexts in which the chlorite crystals have developed.

The material to which chlorite was altered adjacent to the heater was nearly opaque in very dense clusters, but individual flakes were translucent and strongly pleochroic. The pleochroism was deep red-brown parallel to prismatic grains, and yellow-orange across grains; this followed the direction of pleochroism in the unaltered chlorite, which is dark green along prisms and very pale green across. On thin edges of altered chlorite grains, very high birefringence was observed (in contrast to the unaltered chlorite), as well as a somewhat mottled extinction like that of muscovite or biotite.

The heater-induced alteration of muscovite grains consisted of a pale yellow, pleochroic coloration of grain edges which, for very small crystals intergrown with chlorite, extended across whole grains. This alteration was not confined to such a narrow zone around the heater hole as was the alteration of chlorite; it was visible in all thin sections cut from the drillback cores, which cover a distance of approximately 50 cm from the heater hole. The heater-induced muscovite coloration was similar to that typically observed in sericite grains (sericite is a textural designation for fine-grained muscovite of secondary origin) in fractures in both heated and unheated quartz monzonite. This similarity of coloration raised the question of structural or chemical similarity with sericite as well.

The alteration of chlorite and, especially, muscovite in the sample of quartz monzonite heated to 600°C in the laboratory contrasted well with that observed in the drillback cores. Chlorite alteration was similar but more pronounced: aggregates of chlorite grains in thin sections from this specimen were very nearly opaque, and thin translucent edges of grains were rare or lacking. Seen in incident light, the density of reflection of chlorite aggregates was much greater than in the drillback core samples, and areas of metallic reflection could be seen. Muscovite alteration, on the other hand, had progressed to an entirely different state from that in the drillback cores: grains were yellow to orange in color, and strongly pleochroic. Other optical properties indicated fundamental changes in the structure of this muscovite, despite the short period of heating:  $2V$  was very close to  $0^\circ$  (negative), and optic axis figures showed strong dispersion, while in normal muscovite, and in muscovite in the drillback cores,  $2V \approx 30-40^\circ$  (-), and dispersion is minimal. Chemical changes were also apparent, as the strongly

heated muscovite grains were typically clouded, and minute birefringent prisms, 5-10  $\mu\text{m}$  in length, had developed within them.

### 2.1.2 Microfracturing

It was originally hoped that the extent of microfracturing in rock surrounding the heater could be observed in thin section. However, since microfracturing is extremely prevalent in unheated Stripa quartz monzonite, it was usually impossible to tell, on the basis of petrographic evidence alone, what fracturing had been specifically induced by the heater experiment. Several samples were impregnated in dyed epoxy for this purpose, but it still was not generally possible to distinguish heater-induced microfractures from fractures either originally present or induced by drilling and core removal. Sets of open fractures, however, could be seen in thin sections cut from slablike fragments spalled from the walls of the heater hole. These open fractures were roughly parallel to the surface of the fragments (and, therefore, to the axis of the heater hole). Similar open fractures perpendicular to the axes of the drillback cores also could sometimes be seen in thin sections of samples from within 5-8 cm of the heater hole. These open fractures, their orientation, and the tabular shape of the spalled fragments indicated that, at least along planes roughly tangential to the heater-hole axis, microfracturing in a narrow zone of the wall occurred.

In the intensely-heated laboratory sample, microfracturing was pervasive and obvious. Grains of quartz and feldspar were consistently cut with networks of tiny cracks, rendering the rock soft and friable. This marked difference in microcrack abundance between the laboratory-heated and the in situ-heated samples may be related to the lack of confining pressure in the former, and to differences in the rates of pore fluid dissipation.

## 2.2 X-Ray Diffraction Analyses

### 2.2.1 Description of Samples and Sample Preparation

X-ray diffraction analyses of chlorites and muscovites were, in all but one case, obtained from powder patterns. Chlorite samples, which were studied in most detail, were separated from the whole rock by sieving crushed samples to a uniform size fraction. This was followed either by picking individual grains or by bulk separation in a Frantz magnetic separator. Both methods were used to see whether variations between chlorites were due entirely to intersample differences or, in some measure, to inherent variability within the same sample. By picking individual grains, chlorite samples of different morphologies could be analyzed separately to see if their diffraction patterns varied, and to see how each compared with the composite diffraction pattern of magnetically separated chlorite.

Chlorites analyzed included six samples from rock directly adjacent to the heaters--either fragments spalled from the wall of the heater hole, or core samples from within 5 cm of the hole--and two from core samples 11-13 cm and 19 cm from the heater hole. Also analyzed, for comparison, were chlorites from unheated quartz monzonite from four other localities of the Stripa mine, as follows: from core N-1, drilled from the time-scaled drift (Nelson et al., 1979); from ~4.0 m in core OH1 BH E7, drilled from the full-scale drift; from 125.2 m in core DBH V-1, a vertical hole drilled from the 410 m level of the mine; and from a thick chlorite-filled fracture in the ultra-large core from the 360 m level (Thorpe et al., 1980). Chloritic samples from the laboratory-heated quartz monzonite were analyzed for comparison.

Diffraction analyses of muscovite separates from corresponding samples of heated and unheated quartz monzonite were also obtained. Fewer muscovites

were analyzed than chlorites, as muscovite samples had considerably less apparent variation than chlorite samples. Six muscovites were analyzed in all--two from unheated quartz monzonite, two from quartz monzonite adjacent to the heater, and two from the laboratory-heated rock. All were separated from the whole rock by picking individual platelets.

Diffraction samples, after being separated for the chlorite or muscovite fractions, were further ground and sieved to less than 53  $\mu\text{m}$ . Samples were then placed in a capillary tube and photographed in a powder camera, using  $\text{Cu K}\alpha$  radiation with a Ni filter.

## 2.2.2 Diffraction Analyses of Chlorites from the Drillback Cores

2.2.2.1 Powder Pattern Analyses. Powder diffraction patterns of chlorites from quartz monzonite adjacent to the heater differ significantly from patterns obtained from chlorite from the unheated rock. Deviations within individual samples were small relative to the variations between different samples, and consistent patterns of low deviation were obtained from all samples of both unheated and heater-adjacent chlorites. Table 1 shows the average line positions for these two groups, and their relative intensities, compared with the line positions of the minerals to which they correspond, usually chlorite. Since this mineral can vary considerably in composition and in line positions, the lines of two chlorites compositionally similar to the Stripa variety (see Section 2.3) have been included in Table 1.

When the heated and unheated chlorites are compared, it can be seen that many lines shifted positions and changed in relative intensities, while several

Table 1. Diffraction patterns--d spacings (Å)--of chlorite separates.

Unheated Stripa quartz monzonite <sup>a</sup>	Quartz monzonite within 5 cm of heater hole <sup>a</sup>	Reference minerals <sup>b</sup>
13.7 -13.8 (w)	13.5 -13.6 (w)	(a) 14.1 <sup>c</sup> (b) 14.0
7.08-7.09 (s)	7.0 (s)	(a) 7.05 (b) 7.08
4.68-4.70 (w-m)	4.55- 4.60 (vw)	(a) 4.67 (b) 4.68
~4.23 (vw, spotty)	~4.23 (vw, spotty)	qz 4.26 mic 4.22
-	~3.65 (vw)	hem 3.66
3.54 (s)	3.48 (m-s)	(a) 3.52 (b) 3.52
3.34 (s,spotty)	3.34 (s, spotty)	qz 3.34 mus 3.32, 3.34
3.18-3.23 (w-m, spotty)	3.18- 3.23 (w-m, spotty)	pl 3.18, 3.21 mic 3.24, 3.25, 3.26
-	~2.90 (w)	mhm(?) 2.95 ep 2.90
-	2.69- 2.70 (w-m)	hem 2.69 ep 2.69
2.60-2.61 (m-s)	2.60- 2.61 (w)	(a) 2.60 (b) 2.62
2.55-2.56 (m-s)	~2.54 (w, broad)	(a) 2.55 (b) 2.57
2.45 (m)	~2.44 (vw)	(a) 2.45 (b) 2.47
2.38 (m)	~2.39 (vw)	(a) 2.39 (b) 2.41
2.27-2.28 (w-m)	-	(a) 2.27 (b) 2.28
~2.12 (vw)	~2.12 (vw)	qz 2.13
~2.01 (m)	~2.02 (vw)	(a) 2.01 (b) 2.01
1.89 (w)	-	(a) 1.88 (b) 1.89
1.82 (w)	1.82 (vw-w)	(b) 1.83 qz 1.82
-	1.69 (vw)	hem 1.69
1.65-1.67 (w)	1.63 (w)	(a) 1.66 (b) 1.67
~1.55 (s)	~1.54 (vw)	(a) 1.55 (b) 1.56
1.51-1.52 (w-m)	1.51-1.52 (m)	(a) 1.51 (b) 1.52

<sup>a</sup> Letters in parentheses refer to relative line intensities: s-strong; m-medium; w-weak; vw-very weak.

<sup>b</sup> The reference chlorites are (a) thuringite, and (b) bavalite. These chlorites are close in d-spacings, and similar in composition (although richer in Fe and poorer in Mg) to Stripa chlorite. Their diffraction patterns and chemical analyses are taken from the Powder Diffraction File of the American Society for Testing and Materials; file numbers are 21-1227 (thuringite) and 7-166 (bavalite). Other abbreviations are as follows: ep-epidote; hem-hematite; mhm-maghemite; mic-microcline; mus-muscovite; pl-plagioclase; qz-quartz.

<sup>c</sup> The diffraction pattern of a different variety of thuringite (file number 3-67) gives a much closer position for this line, 13.6 Å, than do those of (a) or (b).

lines present in one set of patterns disappeared altogether from the other. The most consistent changes related to shifts in line positions: lines of the heated chlorites generally shifted toward lower d-spacings, indicating a shrinking of the lattice dimensions of chlorite in the heated samples. These line shifts were most pronounced among several of the stronger lines at higher d-spacings, particularly the lines at  $\sim 13.8$ ,  $\sim 7.1$ , and  $\sim 3.5$  Å. The error in reading diffraction lines, which drops off rapidly with decreasing d-spacing (Table 2), was generally much lower than the shifts in line positions and was comparable to them only in the case of the lines at 13.5-13.8 Å. Even then, the two sample sets were quite distinct, with little overlap.

Table 2. Estimated errors in reading of diffraction lines.

<u>d (Å)</u>	<u>error (Å)</u>
14.0	0.2
10.0	0.1
7.0	0.05
3.0	0.01
1.5	0.002

A second observation concerns the lines at 3.65, 2.90, 2.69, and 1.69 Å, which were present in the heated chlorites and absent from the unheated ones. These lines were close to the positions of lines prominent in the patterns of the iron oxide minerals hematite and maghemite. The presence of these minerals was therefore likely, but was not proved unequivocally because the lines were generally weak, and the two that were stronger (2.90, 2.69) were

close to the two strongest lines of epidote, which is locally abundant in the quartz monzonite as a fracture-filling mineral. Also, maghemite, if present, should have had a noticeable effect on the magnetic susceptibility of the chlorite separates (see discussion of the laboratory-heated sample, Section 2.2.3), which remained low in these samples. Nonetheless, the absence of these peaks from the patterns of the unheated chlorites argues that hematite, at least, was intergrown with chlorite in rock adjacent to the heater, and the weakness of the lines attributed to hematite should not be surprising unless this mineral were present in major amounts. (For most minerals, a volume concentration on the order of 10% is necessary to yield much of a recognizable diffraction pattern, although this critical concentration varies greatly with different mineral assemblages and cannot be used as a measure of abundance.)

Other differences between the two sets of chlorite patterns in Table 1 affected most of the lines not already discussed. These differences related either to relative intensities of lines common to both sets of patterns, or to lines present in the patterns of the unheated chlorites but absent in those of the heated ones. The differences were most pronounced for the more prominent lines of the unheated chlorites: those at  $\sim 2.60$ ,  $\sim 2.55$ , 2.45, 2.38,  $\sim 2.01$ , and  $\sim 1.55$  Å. No general rule governing these differences between the two sets of patterns was suggested by the data, and the differences were probably due to alterations of the chlorite lattice relating to specific reflections, possibly the result of disorder in the chlorite structure.

Several lines present at the same d-spacings in both sets of chlorite patterns have been attributed to muscovite, quartz, or feldspar (Table 1).

These lines were generally characterized by spots and streaks of variable intensity caused by reflections of individual grains, as opposed to composites of innumerable grains. This is consistent with their inclusion as impurities in the chlorite separates. Except for the line at 3.34, these lines were usually weak, and the intensity of the 3.34 line is attributable to its being near very strong lines of both muscovite and quartz. In patterns of separates of chlorite platelets, where the chance of intergrown muscovite or other minerals being included was lower than in other samples, the 3.34 line was very much attenuated.

Besides patterns for chlorites from both unheated and heater-adjacent (within 5 cm) quartz monzonite, diffraction patterns for two other chlorite samples from the drillback cores were also obtained. Distances of these samples from the heater hole were 11-13 cm and 19 cm. In both cases, the patterns corresponded closely with the patterns of the unheated chlorites, despite the fact that rock at that distance from the heater had been heated above 300°C. Thus, the alteration of chlorite, as shown in diffraction patterns, was evidently confined to a zone very close to the heater. The chlorite color change (from green to red-brown) was also confined to within 10 cm of the edge of the heater hole and probably, therefore, corresponded to the chlorite alteration interpreted from powder patterns.

2.2.2.2 Single-Crystal Analyses. Hematite, even dispersed in very small quantities among chlorite grains, would tend to give chlorite a red-brown color. The question thus arose whether the strong color change in altered chlorite was actually due wholly to dispersed, submicroscopic hematite. To answer that question, as well as to get an independent determination of the lattice dimensions of the chlorite adjacent to the heater, analyses

of several grains of the altered chlorite were made on a precession camera by Professor A. Pabst of the University of California, Berkeley, Department of Geology and Geophysics. These grains were dark red-brown platelets, 0.2 to 0.5 mm in diameter, that were interleaved with muscovite along its cleavage planes.

The results showed that the platelets were in fact single crystals and did not include dispersed hematite or any other mineral. Any hematite present must therefore have been intergrown with chlorite in its blocky, aggregated form, and the red-brown color of the altered chlorite platelets must have been due to changes in the chlorite structure and composition alone.

The single-crystal analyses established the lattice parameters of the altered chlorite as follows:

$$a = 5.21 \text{ \AA}$$

$$c = 14.00 \text{ \AA}$$

$$\beta \approx 90^\circ$$

They also showed that there was a likelihood of disorder in the stackings of layers perpendicular to the c-axis in the chlorite structure. The determination of the crystallographic angle  $\beta$  as  $90^\circ$  implied a hexagonal or pseudo-hexagonal lattice, and the a and c dimensions of the lattice are therefore given as hexagonal parameters. Chlorite is typically monoclinic, with  $\beta \approx 97^\circ$ , so it is generally necessary to specify the length of the b-axis as well. Unit cell parameters of typical monoclinic "14-Å chlorites" are:

$$a = 5.30\text{-}5.35 \text{ \AA}$$

$$b = 9.2\text{-}9.3 \text{ \AA}$$

$$c = 14.1\text{-}14.3 \text{ \AA}$$

$$\beta \approx 97^\circ$$

Dimensions of chlorites of composition similar to Stripa chlorites (see Section 2.3) commonly fall near the upper ends of the ranges of the a and b parameters, and near the lower end of the range of the c parameter (Deer et al., 1962). Thus, the cell dimensions of the altered chlorite adjacent to the heater were atypically low, as was the angle  $\beta$ . Powder pattern analyses also indicated small cell dimensions for this altered chlorite; but powder patterns do not translate directly into quantitative measures of lattice cell parameters, and attempts to fit cell parameters to the observed line positions in the powder patterns by least squares regression were not notably successful. Working in the other direction--i.e., attempting to calculate what the line positions in the powder patterns should have been, given the cell parameters measured by precession camera--also did not give a particularly close fit to the observed powder patterns.

There were thus some discrepancies between the powder patterns and the single-crystal measurements of the altered chlorite. Furthermore, according to the parameters a and  $\beta$  measured from single crystals, the line at 13.5-13.6 Å in the powder patterns should have been at 14.0 Å. (This line position was also somewhat low, for reasons not clear, in the powder patterns of the unheated chlorites.) These discrepancies notwithstanding, both powder and single-crystal x-ray diffraction analyses agreed qualitatively in determining an atypically small unit cell for the altered chlorite.

### 2.2.3 Diffraction Analyses of Chloritic Samples From Quartz Monzonite Heated in the Laboratory

An interesting contrast to the analyses in Table 1 was provided by the sample of quartz monzonite heated to high temperatures in a laboratory oven. In thin section, chlorite alteration in this rock appeared to be a similar

but more advanced version of the alteration that occurred in rock adjacent to the heater; diffraction patterns, however, showed that chlorite alteration in the two samples was very different. This difference was immediately apparent upon separating the chloritic fraction from the laboratory-heated rock. First, the thin chlorite platelets that were readily separated from crushed samples of both unheated and heater-adjacent rock were not present in samples of the laboratory-heated rock. This suggested that the chlorite platelets originally present had recrystallized and completely lost their tabular form. Second, ground samples of chloritic aggregates from this rock were very magnetic, so much so that only a small fraction of the sample remained after passing a hand magnet over it. By contrast, similar samples from heater-adjacent and unheated rock were only faintly affected by a hand magnet, leaving virtually all of the sample behind. (These samples were, however, sufficiently magnetic to be affected by the Frantz magnetic separator, which uses very small differences in magnetic susceptibility to divide samples.)

Diffraction patterns for the very magnetic fraction of the laboratory-heated rock are summarized in Table 3. This fraction was swept several times with a magnet to eliminate nonmagnetic grains, and the diffraction patterns of the resulting sample were composed, with one exception, entirely of lines that were readily correlated with iron oxide or hydroxide minerals. (The exception was the very weak line at  $\sim 3.32$  Å. This line, or one very close to it, was persistent in the chlorite patterns summarized in Table 1, and was probably due to muscovite or quartz.)

The relevant iron oxide minerals are hematite,  $\alpha$ -Fe<sub>2</sub>O<sub>3</sub>; maghemite,  $\gamma$ -Fe<sub>2</sub>O<sub>3</sub>, a ferromagnetic polymorph of hematite, structurally similar to magnetite, which is metastable and inverts to hematite at temperatures

Table 3. Diffraction pattern of magnetic fraction from sample of Stripa quartz monzonite heated in laboratory.<sup>a</sup>

d-spacings (Å)	d-spacings of reference minerals (Å)
~3.65 (vw)	hem 3.66
~3.32 (vw)	mus ~3.32; qz 3.34; (lep 3.29)
~2.9 (w, broad)	mhm 2.95
2.68 (m-s)	hem 2.69; goet 2.69
2.51 (s)	hem 2.51; mhm 2.52
2.45-2.50 (m-s, broad)	goet 2.45, 2.49; lep 2.47
2.20 (vw)	hem 2.20; goet 2.19
~2.04 (w, broad)	hem ~2.07; lep 2.09; mhm 2.08
1.84 (m)	hem 1.838; lep 1.848
1.68 (m-s)	hem 1.690; goet 1.694; mhm 1.701
~1.59 (w, broad)	hem 1.596; mhm 1.604
1.48 (m-s)	hem 1.484; mhm 1.474
~1.45 (s, broad)	hem 1.452; goet 1.453; lep 1.449

<sup>a</sup>Abbreviations of minerals are as follows: hem-hematite; mhm-maghemite; goet-goethite; lep-lepidocrocite; mus-muscovite; qz-quartz.

Abbreviations in parentheses are as in Table 1.

over 200-300°C; goethite,  $\alpha$ -FeO-OH, which dehydrates to maghemite, and is a common weathering product of iron-bearing minerals; and lepidocrocite,  $\gamma$ -FeO-OH, a polymorph of goethite, which dehydrates to hematite. Hematite was the dominant mineral in these samples: all its major lines were present in the powder patterns summarized in Table 3, and it accounted for nearly all the stronger lines in those patterns. The presence of the other iron-oxide minerals was less firmly established. Maghemite was almost certainly present, as all its major peaks were represented, although weakly, in the patterns. Also, as the only strongly magnetic mineral of this group, it would account for the magnetic properties of the sample. (The diffraction pattern of magnetite is quite close to that of maghemite, so the presence of magnetite instead of, or in addition to, maghemite is quite plausible. However, the lines of the magnetite pattern all fall at slightly higher d-spacings than do those of maghemite, and the latter give a better fit to the lines in Table 3.) As for the hydrous minerals, goethite was probably present, since most of its major lines were represented, and lepidocrocite was probably absent, by the same criterion.

The diffraction pattern of the other fraction from the laboratory-heated rock--the small portion of the crushed chloritic aggregates not affected by a hand magnet--showed that in fact very little chlorite was left. None of the chlorite lines prominent in Table 1 were present, and the lines were all due instead to quartz, feldspar, muscovite, or hematite. A sequence of alteration of chlorite is thus apparent, running as follows: the unheated-unaltered Stripa quartz monzonite; quartz monzonite adjacent to the heater, in which chlorite was altered and some hematite probably formed; and the quartz monzonite intensely heated in the laboratory, in which chlorite all but

disappeared and hematite became predominant. The other iron oxide and hydroxide minerals present in the laboratory-heated sample were probably stepping stones on the way to hematite, as goethite would tend to dehydrate to maghemite, and maghemite to invert to hematite, as the duration of heating increased.

#### 2.2.4 Diffraction Analyses of Muscovite

Muscovite samples for diffraction analysis were prepared by hand-picking large, plate-like crystals, and it was not difficult in this way to obtain virtually pure muscovite separates. Diffraction patterns of muscovites were obtained from two samples each of unheated quartz monzonite, quartz monzonite adjacent to the heater (within 5 cm), and the laboratory-heated quartz monzonite. The results are presented in Table 4, alongside the corresponding pattern of a reference muscovite.

In contrast to the analyses of chlorites discussed above, differences between analyses of muscovites from unheated rock and from core samples adjacent to the heater were virtually nonexistent in both positions and intensities of lines. These two sets of analyses were therefore placed in the same column in Table 4. Nearly all of their lines fit well with the positions and relative intensities of lines in the reference muscovite pattern. The color change on the margins of muscovite grains seen in all thin sections of drillback core samples did not affect the diffraction patterns.

The patterns of muscovites separated from the laboratory-heated sample, on the other hand, differed significantly from those of the other two sample

Table 4. Diffraction patterns--d-spacings (Å)--of muscovite separates.

Laboratory-Heated Sample <sup>a</sup>	Unheated Rock and Drillback Cores	Reference Muscovite <sup>b</sup>
* 10.09-10.12 (m)	10.02 (s)	9.95
* 5.03 (vw)	5.00-5.01 (w)	4.97
4.50 (s)	4.48 (s)	4.47
4.31-4.33 (w)	4.31 (w)	4.30
~4.1 (vw)	~4.12 (vw)	4.11
3.91 (m)	3.89 (m)	3.88
* 3.79 (m)	3.72 (m)	3.73
3.51 (m)	3.50 (m)	3.49
* 3.35 (m-s)	3.33-3.34 (s)	3.32, 3.34
3.21-3.22 (m)	3.20-3.21 (m)	3.20
3.01-3.02 (w-m)	2.99-3.00 (m-s)	2.99
2.87-2.88 (w-m)	2.86-2.87 (m)	2.86
~2.81 (vw)	2.79-2.80 (m)	2.79
* ~2.63 (vw)	-	-
2.60 (s)	2.60 (m)	2.60
2.56-2.57 (w)	2.56 (s)	2.57
* 2.51-2.52 (w-m)	~2.50 (vw)	2.49, 2.51
* -	2.46-2.47 (w-m)	2.47
* 2.41-2.42 (w-m)	2.38 (m-s)	2.38
* 2.26-2.27 (m)	2.25 (w-m)	2.25
* 2.16 (w-m)	2.14-2.15 (m-s)	2.13, 2.15
2.08-2.09 (w-m)	2.06-2.07 (vw)	2.05, 2.07
1.99 (m)	1.98-1.99 (m)	1.993
~1.72 (vw)	1.70-1.71 (vw)	1.699, 1.704
* 1.66-1.67 (vw)	1.66 (w)	1.662
~1.64 (w-m)	~1.65 (m-s)	1.646
~1.62 (w)	~1.60 (w-m)	1.603
1.56-1.57 (w)	1.56 (w)	1.559
* 1.53-1.54 (w-m)	1.52-1.53 (vw)	1.524
* 1.51 (w-m)	1.50 (s)	1.504

<sup>a</sup>Asterisked lines fit reported patterns of biotites or phlogopites more closely than muscovite patterns.

<sup>b</sup>Reference muscovite is 2M<sub>1</sub> muscovite, diffraction file number 6-0263.

Notes in parentheses are as in Table 1.

groups. Nearly all lines shifted to somewhat higher d-spacings, indicating an expansion of the crystal lattice, and many lines also changed in their relative intensities. In fact, almost half the lines more closely fitted the diffraction patterns of phlogopites or biotites than reported muscovite patterns, and these lines have been marked with an asterisk in Table 4. It is possible, therefore, that some muscovite had altered to a phlogopite-like mineral (Mg or Fe moving into sites occupied originally by Al), perhaps in fine sheets perpendicular to the c-axis. Intergrowth of a relatively small amount of such a mineral could account for the changes in optical properties of muscovites in this sample, which resembled those of phlogopite and biotite with regard to pleochroism and 2V (see Section 2.1.1). Such an intergrowth is chemically plausible, as there is sufficient Mg and, especially, Fe in Stripa muscovites (see Section 2.3, below).

### 2.3 Electron Microprobe Analyses

Chemical analyses of chlorites and muscovites by electron microprobe were obtained on three samples from the drillback cores near the heater hole, and on the sample of quartz monzonite heated in the laboratory. The drillback core samples were from the interval between 6 and 10 cm from the edge of the heater hole. In this interval, the transition from unaltered green chlorite to altered red chlorite occurred. Samples were analyzed for eight oxides--Na<sub>2</sub>O, TiO<sub>2</sub>, K<sub>2</sub>O, MgO, SiO<sub>2</sub>, FeO, CaO, and Al<sub>2</sub>O<sub>3</sub>--and analyses were obtained on the electron microprobe at the Department of Geology and Geophysics, U.C. Berkeley.

#### 2.3.1 Microprobe Analyses of Chlorites

A summary of the microprobe analyses of chlorites is given in Table 5. The table also compares these analyses with microprobe data (four major oxides

Table 5. Mean chlorite analyses by electron microprobe.<sup>a</sup>

Oxide	Unheated quartz monzonite, N-1 core time-scaled drift (30 points)	Drillback core samples <sup>b</sup>			Quartz monzonite heated in the laboratory (12 points)
		~10 cm (7 points)	~8 cm (20 points)	~6 cm (17 points)	
Na <sub>2</sub> O	n.a.	<0.05	<0.05	<0.05	0.63 ± 0.18
TiO <sub>2</sub>	n.a.	<0.05	<0.05	<0.05	0.05 ± 0.07
K <sub>2</sub> O	n.a.	<0.05	0.23 ± 0.28	~0.05	1.74 ± 0.30
MgO	6.25 ± .33	5.59 ± 0.55	4.81 ± 0.19	4.90 ± 0.19	7.62 ± 0.69
SiO <sub>2</sub>	24.99 ± .95	22.98 ± 0.52	23.76 ± 1.35	22.99 ± 0.77	24.74 ± 0.49
FeO <sup>c</sup>	34.27 ± 0.92	36.52 ± 0.77	37.58 ± 0.76	37.98 ± 0.94	37.41 ± 1.09
CaO	n.a.	0.03 ± 0.02	.03 ± 0.03	.02 ± 0.02	0.23 ± 0.24
Al <sub>2</sub> O <sub>3</sub>	19.09 ± 0.65	19.52 ± 0.49	18.85 ± 0.71	18.69 ± 0.68	19.69 ± 0.77
TOTAL	84.6	84.7	85.2	84.6	92.1

<sup>a</sup>Values are in weight %; errors are one standard deviation.

<sup>b</sup>Centimeter figures reflect distance of sample from heater hole; figures in parentheses indicate number of points averaged.

<sup>c</sup>All Fe computed as FeO.

only) obtained previously on a sample of unheated quartz monzonite from core N-1 in the time-scaled drift (Wollenberg et al., 1980).

The data in Table 5 are averages, for each sample, of point analyses that were reasonably consistent; the number of averaged points is noted at the head of each column. Many more points were analyzed but not included in Table 5, as difficulties in visually determining grain boundaries on the microprobe often made it unclear whether a particular analysis represented a single grain or a composite intergrowth. For this reason, the consistency of the analyses had to be used as a criterion for inclusion in the Table 5 averages.

Chlorites of different morphological types--densely intergrown aggregates and individual platelets--were sometimes also difficult to distinguish optically, but when they could be, they did not show any consistent differences in chemical composition. Fractures, however, were generally distinguishable, and analyses of fracture-filling chlorites in the three drillback samples indicated that these differed slightly in composition from nonfracture chlorites in those samples. They contained somewhat more MgO, and less FeO (by a little over one standard deviation in each case) than nonfracture chlorites. They also contained measurable, and highly variable, amounts of K<sub>2</sub>O; it may have been deposited on grain boundaries or cleavages by water moving in the fractures. (The high average K<sub>2</sub>O value in the sample at ~8 cm resulted from several analyses of fracture chlorites being included in that average.)

As seen in Table 5, differences among the three drillback samples in the abundances of the major oxides were generally minor and within the listed

error (one standard deviation) in the data. Differences that did appear could not in general be correlated with distance from the heater, even though chlorite alteration was strongly related to distance from the heater in the core interval from which these samples were taken. (A trend is possible in the FeO values, which increased with decreasing distance from the heater, but, again, these differences were barely greater than one standard deviation.)

In comparisons of these chlorite analyses with those of the unheated chlorite from the N-1 core, significant differences did appear with regard to all the major oxides except  $Al_2O_3$ . The unheated chlorites contained more  $SiO_2$  and  $MgO$ , and less  $FeO$ , than did chlorites from the drillback cores. Nonetheless, the totals were about the same in both sets of chlorite analyses, indicating that there was no appreciable loss or gain of  $H_2O$  in the drillback chlorites despite heating above  $300^\circ C$ . (This analysis assumes that all iron was in the ferrous state. If an appreciable amount of iron were present as  $Fe_2O_3$ , this would raise the oxide sum, indicating a lower weight percent of  $H_2O$ .)

The chemical composition of chlorites from the sample heated in the laboratory was quite different from that of the other chlorites in Table 5. (The data from this sample are referred to as analyses of chlorite, even though, as will be discussed later, x-ray diffraction analyses show that very little chlorite may have been present there.) The total of analyzed oxides was much higher, indicating, as would be expected, a significant loss of  $H_2O$ . Differences in the abundances of the four major oxides were also clear, and are brought into sharper focus when normalized to 100% total oxides. Chlorite in this sample then contained 42% more  $MgO$ , and 8% more

FeO, than did chlorites from the drillback cores on the average; these abundances were in fact much closer to those of the unheated chlorites. The normalized abundances of the other two major oxides, SiO<sub>2</sub> and Al<sub>2</sub>O<sub>3</sub>, were lower in the laboratory-heated sample than in the drillback samples, but the differences were on the order of one standard deviation.

Large differences in the minor oxide abundances also occurred between chlorites from the laboratory-heated rock and those from other samples. In the former, K<sub>2</sub>O and, to a lesser extent, Na<sub>2</sub>O were substantially higher, reaching a level that is rarely, if ever, found in naturally occurring chlorites (Deer et al., 1962); CaO also was higher, although less consistently, while TiO<sub>2</sub> remained very low. A possible source of the added K<sub>2</sub>O may have been muscovite, with which chlorite was commonly intergrown, and which was depleted in K<sub>2</sub>O in the laboratory-heated sample (see Section 2.3.2). The increments in Na<sub>2</sub>O and CaO may have been due to residual water left in fractures and cracks which vaporized upon heating; this is plausible as the two major cations present in groundwater at the level of the heater experiment were Na<sup>+</sup> and Ca<sup>++</sup> (Fritz et al., 1979). A derivation of K<sub>2</sub>O, Na<sub>2</sub>O, and CaO from feldspar is also plausible but less likely, as feldspars in this sample did not appear to be depleted in these oxides relative to feldspars in the other four samples analyzed.

In Table 6A, the chemical analyses presented in Table 5 as oxide weight percentages are recalculated as ionic abundances, based on oxygen as the sole anion and on a total of 36 oxygen atoms. The amount of structural H<sub>2</sub>O was taken arbitrarily as 11 wt. % for chlorite from the drillback cores and from unheated rock (a value typical of published chlorite analyses, Deer et al.,

Table 6. Mean ionic abundances (A) and structural formulas (B) of chlorites analyzed by microprobe.<sup>a</sup>

A.	Unheated N-1 core	Drillback cores			Laboratory-heated sample
		~10 cm	~8 cm	~ 6 cm	
Na	-	<0.01	< 0.01	<0.01	0.30 ± 0.07
Ti	-	<0.01	< 0.01	<0.01	<0.01
K	-	<0.02	0.07 ± 0.07	< 0.03	0.57 ± 0.07
Mg	2.16 ± 0.15	1.90 ± 0.19	1.64 ± 0.06	1.68 ± 0.10	2.87 ± 0.20
Si	5.69 ± 0.16	5.25 ± 0.09	5.42 ± 0.21	5.30 ± 0.14	6.35 ± 0.10
Fe	6.52 ± 0.15	6.97 ± 0.12	7.17 ± 0.15	7.32 ± 0.13	7.90 ± 0.18
Ca	-	<0.01	<0.01	<0.01	0.06 ± 0.05
Al	5.04 ± 0.16	5.16 ± 0.08	5.08 ± 0.15	5.08 ± 0.17	5.94 ± 0.18
OH	16.60 ± 0.16	16.75 ± 0.12	16.75 ± 0.19	16.92 ± 0.16	6.20 ± 0.06

B.

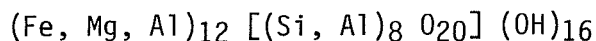
Unheated N-1 core  $(\text{Fe}_{6.52} \text{Mg}_{2.16} \text{Al}_{2.73}) [(\text{Al}_{2.31} \text{Si}_{5.69}) \text{O}_{19.40}] (\text{OH})_{16.60}$   
11.41

Drill-back cores {  
 ~10 cm:  $(\text{Fe}_{6.97} \text{Mg}_{1.90} \text{Al}_{2.51}) [(\text{Al}_{2.75} \text{Si}_{5.25}) \text{O}_{19.25}] (\text{OH})_{16.75}$   
 11.38  
 ~8 cm:  $(\text{Fe}_{7.17} \text{Mg}_{1.64} \text{Al}_{2.50}) [(\text{Al}_{2.58} \text{Si}_{5.42}) \text{O}_{19.25}] (\text{OH})_{16.75}$   
 11.31  
 ~6 cm:  $(\text{Fe}_{7.32} \text{Mg}_{1.68} \text{Al}_{2.38}) [(\text{Al}_{2.70} \text{Si}_{5.30}) \text{O}_{19.08}] (\text{OH})_{16.92}$   
 11.38

Laboratory-heated sample  $(\text{Na}_{.30} \text{K}_{.57} \text{Fe}_{7.90} \text{Mg}_{2.87} \text{Al}_{4.29}) [(\text{Al}_{1.65} \text{Si}_{6.35}) \text{O}_{29.80}] (\text{OH})_{6.20}$   
15.93

<sup>a</sup>Data calculated from the analyses in Table 5, on the basis of 36 oxygens, 8 ions in tetrahedral sites, and all Fe as FeO. Weight % H<sub>2</sub>O taken as 11.0% in the first four samples, and as 3.7% in the last sample.

1962) and as 3.7 wt. % for chlorites from the laboratory-heated rock to bring the the total weight percent to about the same value in all samples. Structural formulas based on these ionic abundances--and on the assumptions that all iron is FeO and that the number of tetrahedral sites is fixed at eight--are given in Table 6B for the five average chlorite analyses. Chlorites from the drillback cores and the unheated rock were high-FeO, low-MgO chlorites which, when compared with the idealized chlorite formula--



--showed a deficit, at ~11.4, in the number of occupied octahedral sites. (The ratio of OH to O is a function of the arbitrarily chosen abundance of H<sub>2</sub>O.)

There is an apparent discrepancy between the microprobe and the x-ray diffraction analyses of chlorites from the drillback cores. Diffraction patterns of altered chlorites closest to the heater showed distinct shrinkage of the crystal lattice parameters relative to unaltered chlorites, a structural alteration that generally correlates with a decrease in the amount of FeO in chlorite (Deer et al., 1962). But the microprobe data showed that there had instead been an increase in FeO, compared with chlorites from the unheated rock of the N-1 core. This discrepancy may be reconciled by concluding, from the diffraction analyses, that small amounts of hematite probably formed in conjunction with chlorite alteration in the rock adjacent to the heaters. The microprobe analyses of these chlorites may thus include points that were composites of chlorite and fine-grained intergrown hematite, so that some of the FeO in these analyses may have been in hematite rather than in chlorite. The actual ionic abundances of FeO in these chlorites would then have been lower than those given by the structural formulas in Table 6B (accompanied by a corresponding increase in the ionic abundances of the other elements)

and could reflect an actual loss of FeO, compared with chlorites from the unheated rock.

In the case of the laboratory-heated sample, the structural formula in Table 6B probably means very little. The evidence from x-ray diffraction analyses shows that probably very little chlorite remained in that sample, and that much of the FeO originally present had gone to form hematite and other oxides and/or hydroxides. That the microprobe data resemble chlorite analyses is probably due more to the fact that the chemical components had not moved far from their original locations in chlorite than to their presence within a chlorite structure. The microprobe analyses thus represent composites of minute grains recrystallized from chlorite and probably, also, of pigmentary coatings on grain surfaces formed as residues from vaporized interstitial water. (See earlier discussion of added Na<sub>2</sub>O and CaO in this sample.)

### 2.3.2 Microprobe Analyses of Muscovites

Microprobe analyses of muscovites from the four samples already discussed--three from the drillback cores and one heated in the laboratory--are presented in Table 7. No analyses of muscovites from unheated rock were obtained. As was done for chlorite, the results were averaged over all relatively consistent point analyses of muscovites in each sample.

One aim was to see whether the yellow coloration of the edges of muscovite grains in the drillback cores could be correlated with chemical changes. To this end, traverses were made across relatively coarse muscovite grains to observe their chemical variability. These traverses did not show any consistent changes in the major oxide components of muscovite, but did show a definite trend toward increasing TiO<sub>2</sub> and MgO from the centers to the edges

Table 7. Mean muscovite analyses by electron microprobe.<sup>a</sup>

Oxide	Drillback core samples <sup>b</sup>			Quartz monzonite heated in the laboratory (22 points)
	~10 cm (7 points)	~8 cm (19 points)	~6 cm (23 points)	
Na <sub>2</sub> O	0.10 ± 0.02	0.21 ± 0.07	0.13 ± 0.03	0.74 ± 0.16
TiO <sub>2</sub>	0.13 ± 0.07	0.15 ± 0.04	0.24 ± 0.15	0.19 ± 0.05
K <sub>2</sub> O	10.64 ± 0.25	10.81 ± 0.44	11.11 ± 0.24	9.64 ± 0.48
MgO	1.00 ± 0.14	0.80 ± 0.12	0.94 ± 0.11	0.72 ± 0.06
SiO <sub>2</sub>	45.10 ± 1.02	45.07 ± 0.56	45.27 ± 0.67	46.00 ± 1.59
FeO <sup>c</sup>	3.92 ± 0.17	4.19 ± 0.24	4.54 ± 0.28	4.31 ± 0.20
CaO	0.02 ± 0.02	0.02 ± 0.02	0.02 ± 0.02	0.04 ± 0.06
Al <sub>2</sub> O <sub>3</sub>	28.86 ± 7.8	29.18 ± 0.60	28.06 ± 0.73	32.68 ± 1.42
TOTAL	89.8	90.4	90.3	94.3

<sup>a</sup>Values in weight %; errors are one standard deviation.

<sup>b</sup>Centimeter figures reflect distance of sample from heater hole; figures in parentheses indicate number of points averaged.

<sup>c</sup>All Fe computed as FeO.

of grains. Values of  $TiO_2$  which, in the interiors of muscovite grains, were usually comparable to those of the mean muscovite analyses, commonly doubled near grain edges.  $MgO$  values also increased on the order of 25% from interiors to edges of muscovite grains, a variation that spans roughly one standard deviation to either side of mean muscovite  $MgO$  values.  $FeO$  also may have shown an increase at grain edges, but there was no evidence of consistent trends across grains.

Fine-grained muscovites occurring in fractures--i.e., sericites--in the drillback core samples generally were slightly different from other muscovites, and less consistent, in chemical composition.  $MgO$ ,  $SiO_2$ , and  $FeO$  averaged higher in the sericites, while  $Al_2O_3$  was lower; these differences were on the order of one standard deviation, except for  $MgO$ , which was about two standard deviations. Among nonfracture muscovites from the drillback cores, differences were also apparent between relatively coarse grains and finer grains intergrown with chlorite. The latter contained appreciably greater  $FeO$  and  $TiO_2$ , by 1.5 to 2 standard deviations in each case.

The averaged muscovite analyses in Table 7 show that differences in oxide abundances among the three drillback samples generally fell within the range of one standard deviation. The high values of  $FeO$  and  $TiO_2$  in the sample ~6 cm from the heater hole were probably due to a predominance of fine muscovite grains intergrown with altered chlorite, since fine grains, as mentioned above, had higher values of these oxides than did coarser ones. However, as this sample was closest to the heater, and as the  $FeO$  values increased regularly in the three samples, a correlation with

distance from the heater cannot be ruled out. The values of  $K_2O$  in the three samples similarly increased with decreasing distance to the heater, but no explanation in terms of grain morphology can be offered for this increase. Thus, although x-ray diffraction analyses of muscovites from various distances from the heater were virtually identical, the  $K_2O$  values of muscovites, and possibly the  $FeO$  values as well, suggest some chemical variation with distance from the heater.

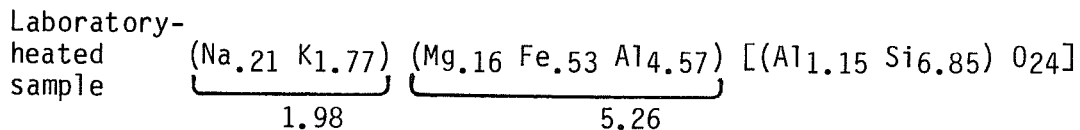
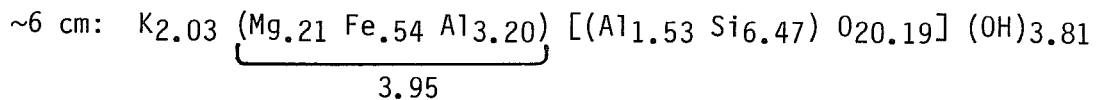
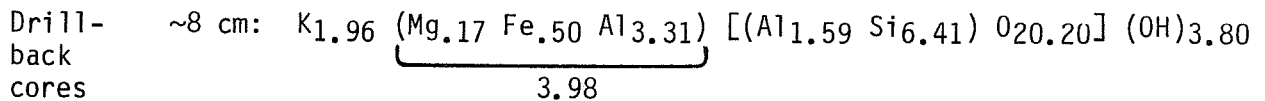
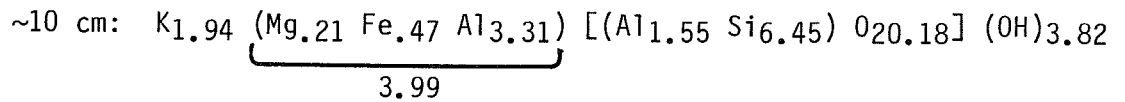
The microprobe analyses of muscovites in Table 7 were recalculated in terms of ionic abundances, and the results are presented in Table 8A, with the corresponding structural formulas in Table 8B. As with chlorites, these calculations assume that iron is in the ferrous state, that oxygen is the sole anion, and that the number of tetrahedral sites is fixed at eight. In this case, the total number of oxygen atoms was taken as 24. A value of 4 wt. % structural  $H_2O$  was used; this value is typical of published muscovite analyses (Deer et al., 1962), but is probably low for the muscovites in this study, as their total oxides averaged only 90.3 wt. %.

By comparing the structural formulas of muscovites from the drillback cores with the idealized muscovite formula-- $K_2Al_4[Al_2 Si_6 O_{20}] (OH)_4$ --it is seen that, in these muscovites, the number of  $K^+$  ions is very close to that of the ideal, but also that there is significant substitution of  $Mg^{2+}$  and, especially,  $Fe^{2+}$  (or  $Fe^{3+}$ ) for  $Al^{3+}$  in octahedral sites, as well as substitution of  $Si^{4+}$  for  $Al^{3+}$  in tetrahedral sites. (The ratio of OH to O is simply contingent upon the arbitrary choice of  $H_2O$  content, which in these muscovites was probably too low.) The term "phengite" is used to denote muscovite with these substitutions for  $Al^{3+}$  in octahedral and tetrahedral sites (Deer et al., 1962). Normally, phengites are fine-grained

Table 8. Mean ionic abundances (A) and structural formulas (B) of muscovites analyzed by microprobe.<sup>a</sup>

A.	Drillback cores			Laboratory-heated sample
	~10 cm	~8 cm	~6 cm	
Na	0.03 ± 0.01	0.06 ± 0.02	0.04 ± 0.01	0.21 ± 0.04
Ti	0.01 ± <0.01	0.02 ± 0.01	0.02 ± 0.01	0.02 ± <0.01
K	1.94 ± 0.05	1.96 ± 0.08	2.03 ± 0.05	1.77 ± 0.08
Mg	0.21 ± 0.04	0.17 ± 0.03	0.21 ± 0.03	0.16 ± 0.01
Si	6.45 ± 0.12	6.41 ± 0.07	6.47 ± 0.08	6.85 ± 0.09
Fe	0.47 ± 0.02	0.50 ± 0.03	0.54 ± 0.03	0.53 ± 0.02
Ca	<0.01	<0.01	<0.01	<0.01
Al	4.86 ± 0.11	4.90 ± 0.10	4.73 ± 0.11	5.72 ± 0.14
OH	3.82 ± 0.05	3.80 ± 0.03	3.81 ± 0.04	0

B.



<sup>a</sup>Samples are as in Table 7. Data are calculated on the basis of 24 oxygens, 8 ions in tetrahedral sites, and all Fe as FeO. Weight % H<sub>2</sub>O is taken as 4% in the first 3 samples and as 0% in the last sample.

muscovites and so fall into the category of sericite. Muscovites in this study, however, had the chemical characteristics of phengite regardless of grain size, although fine-grained muscovites, particularly in fractures, did exhibit these characteristics more strongly.

Mean chemical analyses of muscovites from the sample heated to high temperatures in the laboratory are given in Table 7, where major differences between these and the other muscovites are apparent. The largest differences occurred in the total weight percent oxides, which was much increased in this sample due to loss of  $H_2O$ , and in the  $K_2O$  and  $Al_2O_3$  values. When the analyses were normalized to 100% total oxides,  $K_2O$  in muscovites in this sample decreased by more than three standard deviations over  $K_2O$  in muscovites in the drillback cores;  $Al_2O_3$  increased by a comparable amount,  $Na_2O$  increased by a factor of four, and  $MgO$  and  $SiO_2$  decreased by well over one standard deviation. Traverses across relatively coarse muscovite grains in this sample did not reveal consistent tendencies of any components to increase or decrease toward grain edges, although several, notably  $SiO_2$  and  $Al_2O_3$ , showed a great deal of variability across grains.

The significance of these chemical changes in the laboratory-heated sample is difficult to interpret since, as with the chlorite in this sample, muscovite had probably been extensively recrystallized, and use of the term "muscovite" should be regarded more as a matter of convenience than as a true description of mineralogic composition. (The structural formula given in Table 8 for this "muscovite"--computed on the assumption of 0%  $H_2O$ , which keeps the total weight percent oxides about equal in all the muscovites--may therefore mean little.) Some recrystallization of muscovite in this sample

was observed in thin section, which would be expected, given the stability field of the mineral. At atmospheric pressure, muscovite in the presence of quartz becomes unstable at temperatures above 500°C (monomineralic muscovite remains stable to slightly higher temperatures), breaking down by various possible reactions in which feldspar is formed and water is released (Deer et al., 1962). But even though this sample was heated to 600°C, the breakdown of muscovite was only partial, and on a very fine scale, because of the brief period of heating. This was apparent from the optical and x-ray diffraction evidence, which showed that muscovite--albeit structurally modified, and possibly altered to some degree to a biotite-phlogopite-type mineral--was still a major constituent of the rock.

#### 2.4 Alpha-Radiographic and Gamma-Spectrometric Analyses

The Stripa quartz monzonite is characterized by an abundance of radioelements that is unusually high for such rock. Wollenberg et al. (1980) presented extensive gamma-spectrometric measurements of whole-rock uranium, thorium, and potassium in the quartz monzonite and discussed typical modes of uranium occurrence in the rock, as studied by fission-track radiography of petrographic thin sections. In the present study, the abundance and distribution of radioelements in the drillback cores and in unheated rock were investigated by alpha-radiographic and gamma-spectrometric analyses. This information was compared with the earlier findings to determine whether there was evidence for migration of radioelements from typical locations observed in unheated quartz monzonite, due to heating or heater-induced flow of water in fractures.

#### 2.4.1 Alpha Radiography

The distribution of uranium and thorium in samples from the drillback cores and in several samples of unheated quartz monzonite was studied by alpha radiography of uncovered thin sections. Transparent sheets of cellulose nitrate, sensitive to alpha particles with energies below 4 MeV, were mounted directly on uncovered thin sections, registering the tracks of alpha particles emitted by decay of uranium and thorium (as well as by elements in the uranium and thorium decay series). The alpha detectors were fixed in contact with the rock for 4 weeks, after which they were etched in hot NaOH to enhance the tracks of the alpha particles. The detectors were then remounted over the thin sections in order to view the tracks and the sections in the same microscopic fields, and thus to provide mappings of U-Th loci in the thin sections.

Mappings of two larger segments of the drillback cores, up to 15 cm in length, were also obtained by placing the alpha detectors directly on the surfaces formed by cuts parallel to the core axes. This provided an overview of U-Th locations, particularly along continuous fractures, but not a simultaneous viewing of both detectors and rock on a microscopic scale.

The alpha detectors were the materials CN 85 and LR 115 Type II, discussed by Basham and Easterbrook (1977), and by Duane and Williams (1980). (The detector CN 85 is a more recent version of CA80-15, discussed in the latter paper, from which it differs in color only.)

A total of 14 uncovered thin sections from the drillback cores, in sequences of increasing distance from the heater, were mapped by alpha

radiography, as were the two more continuous segments of the cores described above. Direct comparison of these data on the heated rock with the fission-track radiography data obtained by Wollenberg et al. (1980) on the unheated rock was hampered by two basic problems. First, the typical U-Th loci showed considerable variability in concentration, sometimes even within individual thin sections. To determine whether changes caused by heating had occurred, estimates of the inherent variabilities in concentration of the various types of U-Th sites, in both the heated and unheated rocks, had to be made. These estimates were necessarily qualitative, as the number of instances of any given type of site which were mapped by fission or alpha tracks was usually small.

The second problem was that the alpha exposures, which registered combined uranium and thorium alpha emissions, were not directly comparable to the earlier fission-track exposures, which registered uranium emissions alone. In both cases, standard glasses of known uranium content (and lacking thorium) were exposed, along with the rock samples, to the particle detectors, but the standards could be used to quantitatively measure only the uranium concentration in the fission-track exposures. (Concentrations were measured by comparing areal track densities, which are proportional to uranium concentration, in the standards and the unknown samples.) No independent thorium standard was available for the alpha-track study, and as there was no way to distinguish alpha tracks due to thorium from those due to uranium, the standard uranium glass could not be used to measure uranium concentrations from alpha exposures of the rock samples.

This difficulty was partly resolved by taking three thin sections of unheated rock already studied by fission track radiography and re-exposing

them to alpha detectors. As the sites and concentrations of uranium in those samples were known, and as the ratio of uranium concentration to alpha-track density was known from alpha radiography of the uranium standard, the density of the remaining tracks due to thorium could be calculated. What was not known, since a thorium standard was lacking, was the ratio of thorium alpha-track density to thorium concentration. However, Basham and Easterbrook (1977) suggest that the ratio for uranium of alpha particle emissions to tracks in the detector is about 1.7 times that for thorium. Therefore, a rough idea of thorium concentration was obtained by taking the ratio of alpha-track density to concentration as that of uranium divided by 1.7.

This method of estimating thorium and uranium concentrations was applicable to those three samples studied by both fission track and alpha track techniques, as well as to other samples with very similar U-Th loci. In most cases, however, separate estimates of uranium and thorium concentrations from alpha exposures were not calculated. Instead, comparisons between radioelement sites in the heated and unheated rocks were made on the basis of the density of total alpha tracks alone, using the exposures from the drillback cores, the three duplicate exposures of unheated rock referred to above, and exposures of four other samples of unheated rock chosen for similarities in likely U-Th sites--particularly in fractures--to those seen in the heated rock. This total density of alpha tracks is described here by the unit "equivalent thorium" (equiv. Th), which denotes the concentration of thorium that would be associated with a given alpha-track density were the concentration of uranium zero. The ratio of alpha-track density to thorium concentration is then taken as that of the uranium standard divided by the factor 1.7. (Although equiv. Th generally bears no particular relation to

actual Th concentration, it may not be far off with respect to certain U-Th sites which, as discussed later, were seen by fission-track radiography to contain very little uranium.)

Fission-track radiography disclosed three typical modes of uranium occurrence in the quartz monzonite (Wollenberg et al., 1980): very fine euhedral metallic opaque grains (~50  $\mu\text{m}$  diam) containing 10-20% U or greater; larger anhedral metallic opaque grains (0.2-0.5 mm diam) containing 1-3% U; and occurrences in which uranium was disseminated in fractures and breccias, or associated with chlorite or muscovite grains, generally in concentrations below 0.5-1% U. Of these uranium-bearing sites, the euhedral opaque grains registered strongly in the alpha detectors, as they had in the fission particle detectors, but their associated track densities were too high to be countable so it was impossible to determine whether these grains had different U-Th concentrations in the heated and unheated rocks. Such a comparison was also impossible for the second category of sites, the anhedral opaque grains, because they occurred more rarely than the other loci, and were not observed at all in the drillback core samples.

The third mode of uranium occurrence--dissemination at relatively low concentrations--proved to be more fruitful for this alpha-radiographic study. As they were most commonly associated with fractures or breccias, these occurrences were more promising locations in which to look for evidence of U-Th redistribution. They were also found to encompass a wider range of concentration and mode of occurrence of uranium or thorium than was suspected from fission-track study alone.

Disseminated uranium and/or thorium were commonly associated in the quartz monzonite with chlorite, usually intergrown with sericite in fractures,

interstices of breccias, and fine discontinuous stringers intersecting muscovite or chlorite grains; and also with epidote, which occurred either as the dominant mineral in fractures and breccia interstices, or as a subordinate component of chlorite-sericite fracture fillings. Quartz and calcite, both common as fracture- and breccia-filling minerals in the quartz monzonite, showed little or no association with uranium or thorium.

One other material was commonly found with these minerals and appeared to be an important factor in determining the U-Th concentrations associated with them. This was an opaque or nearly opaque material with a nonmetallic, diffused, cloudy appearance in incident light. It was usually disseminated among the fracture- and breccia-filling minerals, but it was also found in more discrete, concentrated form. On occasion, it was somewhat translucent and birefringent, resembling sphene, possibly intergrown with epidote. The more common variety was therefore taken to be very fine-grained, altered sphene, and is referred to as such in this report. (It was originally referred to in Wollenberg et al., 1980, as altered epidote.) Other reasonable possibilities are altered (probably metamict, due to included radioelements) monazite, xenotime, or allanite, all of which, except possibly allanite, have been reported in vein occurrences (Deer et al., 1962; Heinrich, 1958) and in pigmentary material.

Concentrations of disseminated uranium and/or thorium in fractures and breccias of the heated and unheated rocks ranged from near zero to as high as 20,000 ppm (2%) equiv. Th. The presence or absence of altered sphene was an important factor affecting U-Th concentrations. Chlorite- and sericite-filled fractures with altered sphene commonly contained 2,000-12,000 ppm

equiv. Th; for fractures without altered sphene, a more typical range was 200-8,000 ppm. Similarly, epidote-filled fractures or breccias with altered sphene commonly contained 2000-10,000 ppm equiv. Th, while others were typically below 5,000 ppm. These data are summarized in Table 9A. An orange-colored, reflective material, probably finely disseminated hematite, was sometimes also associated with relatively high U-Th concentrations.

Disseminated U-Th concentrations tended to be lower in the unheated rock than in similar sites in the samples from the drillback cores. Fracture- and breccia-fillings in the unheated rock, whether predominantly chlorite-sericite or epidote, seldom contained concentrations above 6,000 ppm equiv. Th where altered sphene was present, or above 4,000 ppm where it was absent. Concentrations outside these ranges did occur and sometimes were as high as any found in comparable locations in the heated rock. However, such instances were rare, and it may still be concluded that an enrichment occurred in the concentration of disseminated uranium or thorium in the heated rock of the drillback cores.

Often associated with the disseminated U-Th occurrences were discrete nonmetallic opaque sites; these appeared to be more concentrated accumulations of very fine-grained altered sphene. The distinction between disseminated and discrete sites was not always clearly marked because of gradations in the radioelement-bearing material in all contexts--fractures and breccias as well as grain boundaries, stringers, and cleavage planes. Discrete sites thus differed from disseminated ones more in degree than in kind, and as such provided an upper limit to disseminated U-Th concentrations.

Table 9. Uranium-thorium concentrations in typical sites in heated and unheated quartz monzonite.<sup>a</sup>

A. NONMETALLIC SITES

DRILLBACK CORES

UNHEATED ROCK

1) Disseminated Sites

1) Disseminated Sites

range: 0-2% eq. Th<sup>b</sup>

range: 0-2% eq. Th

typical values:  $\left\{ \begin{array}{l} 0.2 - 1.2\% \text{ eq. Th - chl/ser sites w/alt. sph} \\ 0.2 - 1.0\% \text{ " " - epid sites w/alt. sph} \\ 0.02 - 0.8\% \text{ " " - chl/ser sites w/o alt. sph} \\ <0.5\% \text{ " " - epid sites w/o alt. sph} \end{array} \right.$

typical values:  $\left\{ \begin{array}{l} <0.6\% \text{ eq. Th - chl/ ser or epid sites w/alt. sph} \\ <0.4\% \text{ eq. Th - chl/ser or epid sites w/o alt. sph} \\ \left\{ \begin{array}{l} 0 - 300 \text{ ppm U}^b \\ 0.3 - 0.6\% \text{ Th} \end{array} \right\} \text{ -chl/ser sites w/alt. sph} \end{array} \right.$

2) Discrete Sites

2) Discrete Sites

typical values: 1-5% eq. Th - all sites

typical values:  $\left\{ \begin{array}{l} 1-5\% \text{ eq. Th - all sites} \\ \left\{ \begin{array}{l} 0.1-0.4\% \text{ U} \\ \sim 1.5\% \text{ Th} \end{array} \right\} \text{ - all sites} \end{array} \right.$

B. METALLIC GRAINS

Typical Values, Unheated Rock

	<u>U</u>	<u>Th</u>
euhedral grains:	>10-20%	-
anhedral grains:	1-3%	3-8%

<sup>a</sup>Abbreviations: chl/ser: chlorite-sericite  
epid: epidote  
alt.sph: altered sphene

<sup>b</sup>Concentrations expressed in the unit "eq. Th" are combined U-Th concentrations obtained by alpha radiography alone. For explanation of this unit, see p. 42. Where U and Th concentrations are expressed separately, they were obtained by combined alpha track and fission track radiography.

Concentrations in the discrete sites typically ranged from 1% to 5% or more equiv. Th (Table 9A). Comparison of these sites in the heated and unheated rocks showed no consistent differences between the two, in contrast to the disseminated occurrences. However, such differences in U-Th contents of discrete sites would probably have been missed unless they were on the order of a factor of two or more, because large uncertainties were introduced by the combination of high alpha-track densities and the small size of these discrete sites.

No clear correlations between U-Th concentrations and distance from the heater were apparent among the samples from the drillback cores. The U-Th concentration in any given type of site was highly variable in these samples, as it was in the unheated rock; but, overall, there was no evidence for a progressive increase or decrease in uranium or thorium, with distance from the heater, for any U-Th sites.

Use of both fission-track and alpha-track techniques on three thin sections of unheated quartz monzonite allowed separate estimates to be made of uranium and thorium concentrations in some typical sites, and these are summarized in Table 9. The uranium-bearing euhedral and anhedral metallic opaque grains were well represented in these thin sections, as were the discrete nonmetallic U-Th sites occurring in fractures and stringers, and in association with grains of chlorite and muscovite; less well represented were the more disseminated U-Th nonmetallic sites common in the drillback core samples. (In the classification of typical uranium-bearing sites based on fission-track radiography, the discrete nonmetallic sites were grouped together with the disseminated sites and not described separately. This was because of their relatively low uranium concentrations, which produced sparse

accumulations of associated fission tracks. These sparse tracks did not provide good outlines of the uranium-bearing sites, making it difficult to distinguish discrete sites from disseminated ones. Only with the higher density of associated alpha tracks, due mainly to thorium, could the shapes of the discrete U-Th sites be made out and distinguished from a disseminated pattern.)

The anhedral opaque grains in the thin sections of unheated quartz monzonite typically contained 1-3% U and 3-8% Th; the Th/U ratio ranged from 2 to 15, with 5 to 8 most common. The highly uraniferous euhedral opaque grains usually had alpha-track densities much too high to be counted, so thorium concentrations could not be estimated. The discrete nonmetallic U-Th sites were relatively low in uranium, with concentrations on the order of 0.1-0.4%, while thorium, which ranged from 1-5%, was usually about 1.5%; Th/U was most commonly 3 to 6. Uranium concentrations, in the few places where it occurred in disseminated form--in fractures and breccias with chlorite and altered sphene--appeared to be much lower still, generally several hundred ppm or below, while thorium concentrations were typically 0.3-0.6%.

These estimates of uranium and thorium concentrations, together with previously discussed data on combined uranium and thorium, suggest several questions and interpretations. One concerns the high values of the Th/U ratio in all observed sites except the euhedral opaque grains. These high values, together with the low values for the whole rock ( $\text{Th/U} < 1$ , as discussed in the next section), may indicate--if the thorium values, estimated without benefit of a thorium standard, were not greatly in error--that the high radioactivity of the euhedral opaque grains was due primarily to uranium.

Another, more important question for this study concerns the source of the disseminated uranium or thorium apparently added to the heated rock of the drillback cores. It is not possible to resolve this question definitively from the available data, but two possibilities are most reasonable. One is that the added radioelements were derived from the discrete U-Th sites, which occurred in the same types of settings as the disseminated ones, and which were associated to a large extent with the same reflective, nonmetallic material (altered sphene). While U-Th concentrations of the discrete sites did not appear to be different, overall, in the heated and unheated rocks, differences may well have gone undetected due to lack of sufficient precision in estimating those concentrations. The euhedral opaque grains may also have been sources of disseminated radioelements, but no evidence for or against this hypothesis is available.

Whatever the source or sources may have been, it is likely that the Th/U ratio would have been low at sites where these elements were added by heated fracture waters, as uranium is the more mobile element in aqueous environments. (This would be in contrast to the sites of disseminated uranium or thorium in the unheated rock, which showed high Th/U ratios.) Fission-track radiography of several drillback core samples and exposure of thorium standards to alpha detectors would be valuable in testing this hypothesis and in pinpointing the source of disseminated uranium-thorium added to the drillback core samples.

#### 2.4.2 Gamma Spectrometry

As a supplement to the alpha-radiographic study of uranium-thorium distribution, whole-rock gamma-spectrometric analyses for uranium, thorium,

and potassium were obtained on segments of one drillback core by A. Smith in the LBL low-background counting facility. Nine samples, each between 12 cm and 18 cm in length, were analyzed in all; three were from that portion of the core from which thin sections had been cut, i.e., not more than 70 cm from the heater axis (less than 50 cm from the edge of the hole); the remainder were from distances of 0.5 m to 6.0 m from the heater axis.

Table 10 summarizes the gamma-spectrometric analyses of the drillback cores, as well as mean values of field analyses of the quartz monzonite. The field analyses, taken from Appendix B of Wollenberg et al. (1980), were obtained underground by portable gamma spectrometer and are divided into three groups: (1) all analyses from the 310 m to 360 m levels of the mine; (2) analyses from the experimental area at 330 to 340 m; and (3) analyses specifically from the time-scaled, full-scale, and extensometer drifts in the experimental area, with which the drillback core samples, before heating, should have been most comparable.

Both the field and laboratory gamma-spectrometric analyses are based on accumulated counts in three intervals of the  $\gamma$ -ray spectrum centered at 1.46 MeV, 1.76 MeV, and 2.62 MeV. These intervals correspond, respectively, to the  $\gamma$  peaks of  $^{40}\text{K}$ ,  $^{214}\text{Bi}$ , and  $^{208}\text{Tl}$ . As  $^{214}\text{Bi}$  and  $^{208}\text{Tl}$  are respective daughter products of the  $^{238}\text{U}$  and  $^{232}\text{Th}$  decay series, it is assumed that they are in secular equilibrium with their parents in the rocks being measured.

In Fig. 4, the data presented in Table 10 are plotted with reference to distance from the heater axis. The data from the drillback cores are plotted to the left of the vertical line representing the heater axis. Core segments from either side of the heater hole are plotted together; dashed

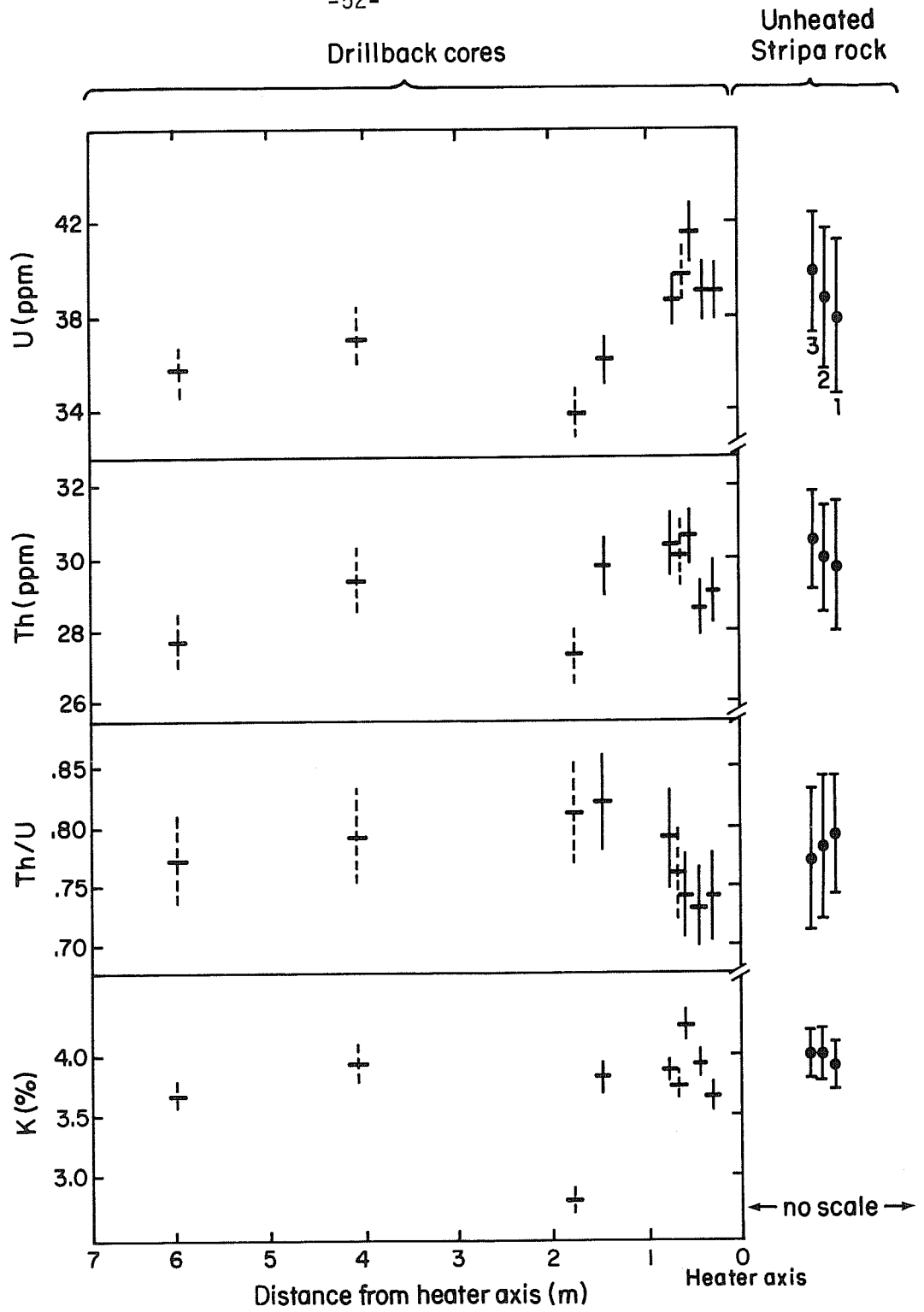
Table 10. Analyses of heated and unheated quartz monzonite samples by gamma spectrometry.

	Distance from heater axis (m) <sup>a</sup>	U (ppm)	Th (ppm)	K (%)	Th/U
Drillback core segments <sup>b</sup>	+0.30	39.2	29.2	3.65	0.74
	+0.44	39.2	28.7	3.91	0.73
	+0.58	41.7	30.7	4.24	0.74
	+0.75	38.8	30.5	3.87	0.79
	+1.45	36.3	29.9	3.82	0.82
	-0.65	39.9	30.2	3.75	0.76
	-1.75	34.0	27.4	2.78	0.81
	-4.05	37.1	29.4	3.93	0.79
	-5.95	35.8	27.7	3.66	0.77
Unheated quartz monzonite <sup>c</sup>	Full-scale, time-scaled, and extensometer drifts (12 analyses)	40.0 ± 2.5	30.6 ± 1.4	4.0 ± 0.2	0.77 ± 0.06
	Experimental area 330-340m levels (19 analyses)	38.9 ± 2.9	30.1 ± 1.5	4.0 ± 0.2	0.78 ± 0.06
	Overall 310-360 m levels (30 analyses)	38.1 ± 3.2	29.9 ± 1.8	3.9 ± 0.2	0.79 ± 0.05

<sup>a</sup>Distance from heater is measured from the middle of the core segments to the heater axis. Sign indicates which side of heater each core segment corresponds to; (-) side is farther from collar of drill hole.

<sup>b</sup>Determined by laboratory analysis. Analytical errors of the individual analyses encompass errors due to counting statistics as well as any systematic errors, and are under 3% for the elemental analyses, and under 6% for Th/U.

<sup>c</sup>Determined by underground  $\gamma$ -spectral analyses, and summarized from Wollenberg et al. (1980), Appendix B. Errors represent one standard deviation of the averaged analyses in each group.



XBL 829-2388

Fig. 4. Variation of U, Th, and K with distance from the H-10 heater and comparison with analyses of unheated Stripa rock.

and solid vertical error bars distinguish samples from these two sides, with dashed bars denoting samples which have a negative distance from the heater axis in Table 10. Horizontal bars indicate lengths of core segments.

Data from the unheated rock are plotted to the right of the vertical heater axis line in Fig. 4. These data are divided into the three groupings used in Table 10, and are numbered accordingly. Errors in the analyses of both the drillback core and unheated rock samples are indicated by the vertical bars in Fig. 4 (both solid and dashed bars are used for the drillback core analyses), and the errors correspond to those in Table 10.

Although the small number of samples of the drillback core analyses prevented any firm conclusions from being drawn, the data in Table 10 and Fig. 4 show the following trends: Uranium abundance was distinctly higher in the samples within 1 m of the heater axis than in those farther from the heater. Thorium values showed a similar, but less distinct trend. The Th/U ratio was lowest near the heater, rose, and then fell to an intermediate value as distance from the heater increased. No correlation of potassium values with distance from the heater was evident.

Comparison of these data with the means and standard deviations of the field analyses of the unheated quartz monzonite provided a guide to the significance of the variations in these drillback core data. (It should be noted that these two sets of data are not strictly comparable, as one set consisted of field measurements, the other of laboratory measurements. But since the former were already corrected for systematic variation from laboratory measurements, discrepancies between the two should be small.) Compared with the deviations in the field analyses, the low uranium values

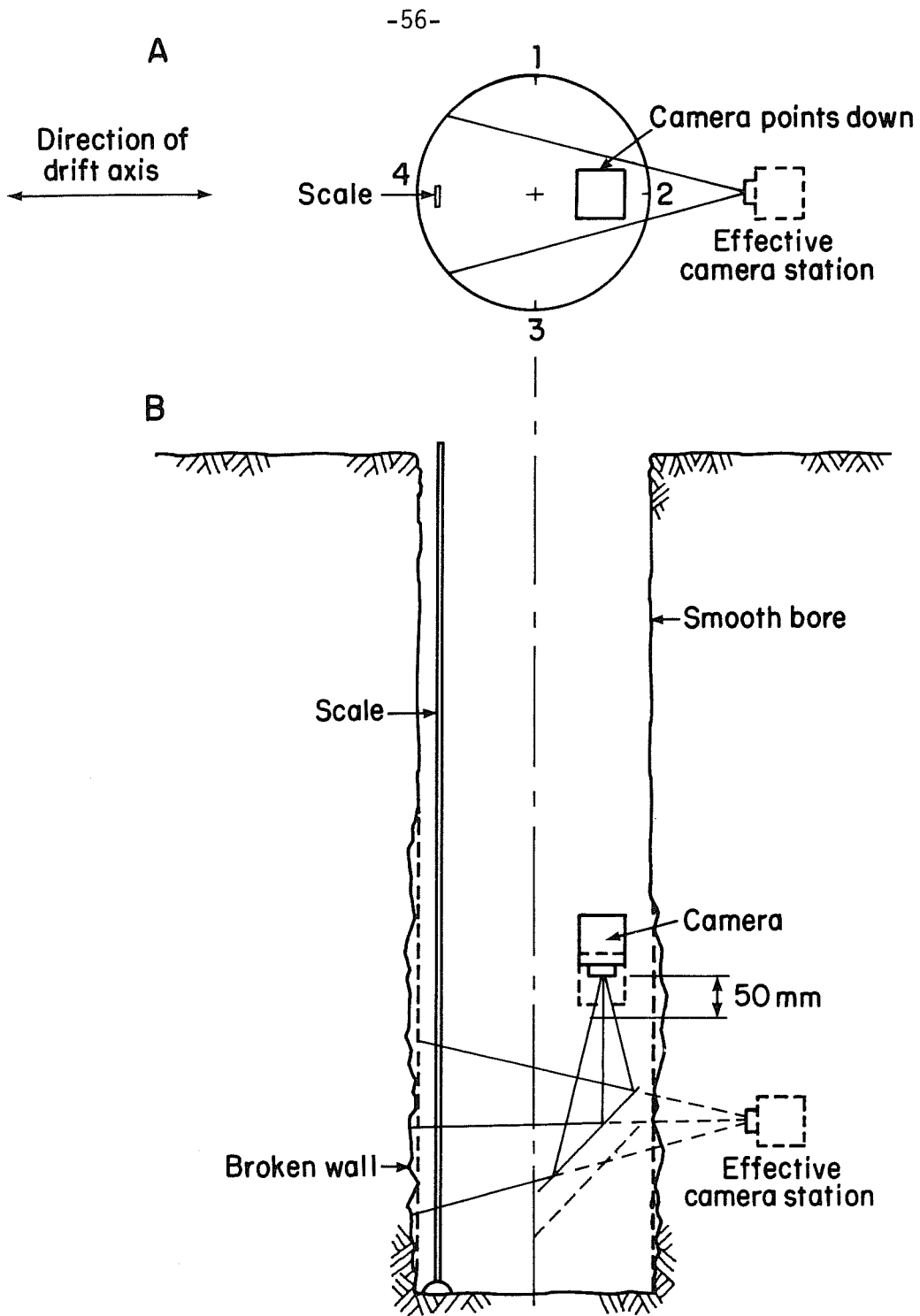
of the samples more distant from the heater were generally within one standard deviation ( $1 \sigma$ ) of the mean of the analyses from the 310-360 m levels overall, but were outside  $1 \sigma$  with respect to the data from the adjacent time-scaled, full-scale, and extensometer drifts. Of the thorium values, only the two lowest were significantly ( $1 \sigma$ ) below the means of the thorium field analyses, and these were low with respect to all three data groups. The variation in Th/U values in the heated rock was not significant, compared with  $1 \sigma$ , with respect to any of the three groups of field analyses; but the lowering of Th/U values nearest the heater hole appeared to be consistent, and so may reflect an actual lowering.

If these trends are real and not merely artifacts of the small number of drillback core samples analyzed, they may indicate migration of uranium (and, to a lesser extent, thorium) toward the heater hole from rock beyond about 1 m from the heater axis. Such migration would probably have been effected by fracture waters responding to the hydrostatic pressure gradient toward the heater hole and would be consistent with the observation, by alpha radiography, of disseminated uranium or thorium apparently added to the rock near the heater. Alpha exposures of thin sections from the drillback core segments more than 1 m from the heater axis ( $>0.7$  m from the heater hole), already analyzed by gamma spectrometry, would be an important follow-up to this study; they would provide a test of the hypothesis, suggested by the whole-rock analyses, that there was a depletion in uranium or thorium in one or several of the typical U-Th sites, at distances  $>1$  m from the heater axis--a depletion that would balance the addition of uranium or thorium at disseminated sites nearer the heater.

### 3. BOREHOLE STEREOGRAPHY

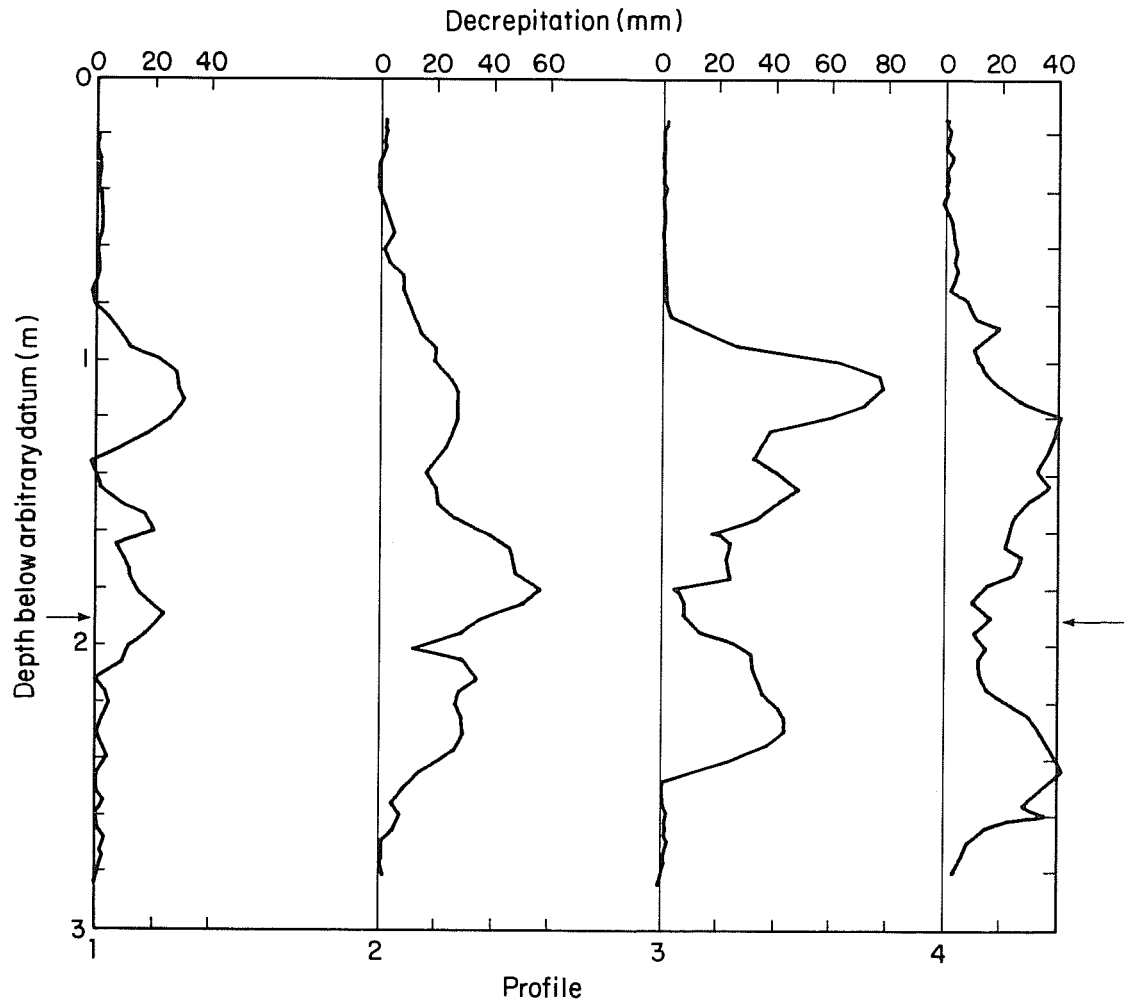
The walls of heater hole H-10 were stereographically photographed after completion of the heater experiment; on the basis of these photographs, calculations were made to determine the extent of decrepitation. The stereo-camera setup in the empty heater hole is shown in Fig. 5, as are the locations of four vertical transect lines. The camera was lowered along these transect lines in successive 50-mm steps from the smooth upper portion of the wall into the decrepitated zone, thus obtaining complete stereophotographic coverage. The degree of decrepitation shown on the vertical profiles in Fig. 6, constructed along the transect lines, was measured photogrammetrically relative to the vertical measuring tape suspended in the hole (Fig. 5). Correction was made for the position of the tape relative to the original smooth wall, giving the depth of decrepitation.

The process of correction and calculation was performed at 5-cm intervals along the four vertical lines down the sides of the hole, resulting in the four decrepitation profiles shown in Fig. 6. The maximum depth of decrepitation, indicated on profile 3, was about 8 cm. The four profiles indicate that most of the decrepitation occurred above the midplane of the heater. The total volume of rock shed from the wall was estimated by assuming that each profile represents the shape of 1/4 of the circumference of the hole; then the area under the curves was integrated over the length of the decrepitated zone. The volume of rock thus computed is  $0.059 \text{ m}^3$ , which gives an average decrepitation depth over the length of the heater of 1.68 cm. Assuming a rock density of  $2.6 \text{ g/cm}^3$ , the mass of decrepitated rock is 153 kg. This compares with 142.4 kg of material actually weighed from the H-10 hole (H. Carlsson, private communication, 1981).



XBL 829-2390

Fig. 5. (A) Plan of H-10 heater hole, showing positions of the four vertical transects corresponding to the profiles in Fig. 6. Camera position is along transect 2. (B) Cross-section of H-10 heater hole, showing camera positioned as in (A) and scale located opposite camera.



XBL 829-2392

Fig. 6. Decrepitation profiles from the H-10 heater hole, located along the positions of the vertical transects shown in Fig. 5A (arrows indicate approximate midplane level of the heater).

The temperature and the induced thermal stress at which gross decrepitation occurred were estimated by Hood et al. (1979). These estimates agreed with the concept that major decrepitation takes place when the maximum tangential or axial stress (calculated to be 215 MPa at the heater midplane) exceeds the uniaxial compressive strength of the rock (measured as  $208 \pm 31$  MPa). Because of the displacements and stresses that this degree of decrepitation would register on the instruments emplaced in the surrounding rock, it is evident that a significant effect would occur only in the very near field around the central heater. Since the nearest extensometer anchor points were at a radius of  $\sim 1$  m from the central heater, and the nearest IRAD USBM stress gauges were at a radius of  $\sim 1.5$  m (Schrauf et al., 1979), it is assumed that the effect of decrepitation on these instruments was negligible. Furthermore, the gross decrepitation did not take place until after the peripheral heaters were turned on, and all the relevant instruments are outside the ring of peripheral heaters. This further decreases the effect on the instrumentation of the relatively small volume of rock around the wall of the heater hole.

Examination of the profiles (Fig. 6) and their locations (Fig. 5) suggests that most of the decrepitation was in the upper portion of the damaged zone. Profiles 1 and 3 in Fig. 6 show sharply increasing depths of decrepitation near the top of the damaged zone, while profiles 2 and 4 show a more gradual increase of decrepitation depth in this zone. This pattern is confirmed by the photographs of the borehole wall. From Fig. 5A, we see that the upper zone of sharp decrepitation is aligned perpendicularly to the axis of the heater drift. This alignment may be influenced by the presence of the drift, but it is not evident deeper in the hole. This suggests that the

geometry of the decrepitated zone is most directly controlled by the fracture pattern, not by the directions of the principal stresses in the intact rock, or by stress distributions associated with the underground galleries. This supposition can only be confirmed by a detailed comparison of the decrepitation with fracture patterns and stress measurements; such a comparison was beyond the scope of this study.



#### 4. SUMMARY AND CONCLUSIONS

The major portion of this study concerned the mineralogic effects of the heater experiment on the rock surrounding the H-10 heater. Investigation focussed on the minerals chlorite and muscovite, which were sampled from various distances from the heater, and studied by petrographic microscope and by x-ray diffraction and electron microprobe analyses.

Chlorite within 10 cm of the edge of the heater hole was altered to a dark red-brown material that was strongly pleochroic and birefringent. Conductive heating of the rock was not the only cause of this alteration; circulating hot water was a contributing, if not a dominant factor, as indicated by the preferential alteration of chlorite near fractures. X-ray diffraction analyses showed that chlorite within ~12 cm of the heater hole had altered significantly from the chlorite found both in unheated rock and in drillback core samples farther from the heater. This alteration took the form of shrinkage of the chlorite crystal lattice, probably combined with intergrowth of fine hematite. The red-brown coloration of the altered chlorite could not be attributed solely to intergrowth of hematite or any other mineral, but must have been due partly, if not mainly, to structural and chemical changes in the chlorite itself. In addition to shrinkage of the chlorite lattice, other structural changes included alteration to a hexagonal or pseudo-hexagonal symmetry, and a likelihood of disorder in the stacking of layers perpendicular to the c-axis.

Chemically, both the altered and unaltered chlorites were shown by microprobe analyses to be high-FeO, low-MgO chlorites. Chlorites from

the drillback cores differed significantly from chlorite from one sample of unheated quartz monzonite, containing less  $\text{SiO}_2$  and  $\text{MgO}$ , and more  $\text{FeO}$ . They did not, however, appear to have been dehydrated relative to the unheated chlorite (this is based on an assumption that iron did not change oxidation state). Little or no evidence was found to suggest chemical variation among drillback core chlorites from the interval between 6 and 10 cm from the edge of the heater hole, the interval in which the transition between altered and mainly unaltered chlorite took place. Some differences were apparent, however, between fine, fracture-filling chlorite and other chlorite in the drillback core samples. The former contained more  $\text{MgO}$  and less  $\text{FeO}$ , as well as measurable and variable amounts of  $\text{K}_2\text{O}$  possibly deposited by circulating water.

Alteration of muscovite in the drillback cores was confined to a faint, yellow, pleochroic coloration of grain margins. This effect, which was only visible microscopically, occurred to distances of at least 50 cm from the heater hole, and resembled the coloration of fine-grained, fracture-filling sericite common in the Stripa quartz monzonite. X-ray diffraction analyses of muscovites showed no discernible differences between muscovites from the drillback cores and unheated muscovites, and the two sets of muscovite samples gave virtually identical diffraction patterns.

Microprobe analyses showed that the drillback core muscovites were high in  $\text{H}_2\text{O}$ , and were phengitic (octahedral  $\text{Al}^{3+}$  replaced by  $\text{Fe}^{2+}$  or  $\text{Fe}^{3+}$ , and by  $\text{Mg}^{2+}$ ; tetrahedral  $\text{Al}^{3+}$  replaced by  $\text{Si}^{4+}$ ) in composition. Muscovites in the interval between 6 and 10 cm from the heater hole were quite uniform in composition, but showed a possible trend toward increase

in FeO and K<sub>2</sub>O in samples close to the heater. Microprobe traverses across muscovite grains showed changes only in the minor oxides TiO<sub>2</sub> and MgO, both of which increased toward grain margins. Fine-grained fracture-filling muscovite (sericite) was less uniform in composition than other muscovites analyzed, and showed a trend toward higher MgO contents.

In addition to the effects on chlorite and muscovite, another change evident in rock near the heater was a lightening in the color of the core, including a slight pink coloration, visible up to 20 cm from the edge of the heater hole. This effect was probably produced by a clouding of feldspar grains, only faintly visible microscopically, which resulted either from oxidation of iron impurities or from minute clay alterations in the feldspar.

Another sample of Stripa quartz monzonite, heated in a laboratory oven to 600°C over 3 weeks, provided a contrast to the mineralogic alterations observed in the drillback cores. Chlorite alteration in this sample took the form of a much darker, nearly opaque, red-brown material than that in the drillback cores. X-ray diffraction analyses showed that chlorite had largely disappeared from this material, which was mainly a composite of iron oxides and hydroxides dominated by hematite, and containing maghemite (or possibly magnetite) and probably goethite. This represented an advanced state of the alteration of chlorite attained in the drillback cores, in which an altered form of chlorite was still dominant, and only a small amount of hematite had formed. Microprobe analyses of these intergrowths of chlorite alteration products, compared with analyses of the other chlorites, indicated dehydration and major increases in MgO, K<sub>2</sub>O, Na<sub>2</sub>O, and, to a lesser extent, FeO and CaO.

Alteration of muscovite in the laboratory-heated sample was also pronounced. Since muscovite is unstable at the pressure-temperature conditions to which this rock was subjected, the presence of any muscovite in this sample is attributable only to the short period of heating. In thin section, muscovite alteration took the form of a strong orange pleochroism, accompanied by a change in 2V, dispersion of the optic axes, and minute recrystallization. X-ray diffraction patterns showed a shift of the muscovite lines, indicating expansion of the crystal lattice, and/or intergrowth of a biotite-phlogopite-like mineral. Development of such a mineral would be consistent with some of the optical properties of the altered muscovite and would indicate a structural reorganization of the Fe and Mg already present. The main changes in the chemical composition of muscovite in this sample were loss of H<sub>2</sub>O, large increases in Na<sub>2</sub>O and Al<sub>2</sub>O<sub>3</sub>, and a large decrease in K<sub>2</sub>O.

The distribution and abundance of uranium and thorium in the drillback cores was studied by alpha radiography, and the results were compared with an earlier study by fission-track radiography to determine whether there was migration of these elements in the heated rock. When typical U-Th sites in the heated and unheated rocks were compared, evidence was found suggesting addition of uranium or thorium to sites of disseminated accumulations of these elements in samples from the drillback cores up to at least 50 cm from the heater hole. These sites of disseminated uranium or thorium included fractures and breccias, and cleavage planes and grain boundaries of chlorite and muscovite grains. They were generally associated with a fine, reflective, nonmetallic material that was most likely an altered form of sphene.

Sources of this added uranium or thorium were not identifiable from the available data. But whole-rock gamma-spectrometric analyses of several drillback

core segments provided some evidence of depletion of uranium, and possibly of thorium, in core more than 70 cm from the heater hole (outside the zone studied by alpha radiography). This suggested that migration of these elements to disseminated sites nearer the heater may have occurred.

Stereophotographic traverses were made in the H-10 hole to document decrepitation of the wall in response to heating. Maximum depth of decrepitation observed was ~8 cm, and the depth averaged 1.7 cm over the length of the heater. Megascopic examination indicated no apparent preferred orientation to the decrepitation attributable directly to stresses in the intact rock mass or to stresses associated with the underground galleries. However, as would be expected, microfracturing oriented tangentially to the heater hole was observed in thin sections of rock spalled from the hole wall. A detailed comparison of decrepitation with fracture patterns and stress measurements, which was beyond the scope of this study, would be necessary to evaluate the influence of stresses and fracturing on decrepitation.



#### ACKNOWLEDGMENTS

Lennart Andersson, now with Statoil, Oslo, Norway, supervised the drilling of the drillback holes. Borehole stereophotography and photogrammetry was done by VIAK, AB, under the direction of Dr. Rolf Larsson. Professor Francis Moffitt of the Department of Civil Engineering, University of California, Berkeley, participated in the planning and evaluation of the photogrammetric program. Alan Smith of LBL provided the gamma-spectrometric analyses of the drillback core segments. Professor Adolph Pabst of the Department of Geology, University of California, Berkeley, performed single-crystal analyses for lattice dimensions of chlorite grains. Electron microprobe scans were made under the guidance of Mark Rivers at the Department of Geology, University of California, Berkeley. Dai Watkins of LBL read the manuscript of this report and provided valuable criticism and suggestions.



REFERENCES

- Basham, I.R. and G.D. Easterbrook, 1977. Alpha-Particle Autoradiography of Geological Specimens by Use of Cellulose Nitrate Detectors. Inst. Mining Metallurgy Trans., V. 86, sec. B., pp. 96-98.
- Chan, T., N. Littlestone, and O. Wan, 1980. Thermomechanical Modeling and Data Analysis for Heating Experiments at Stripa, Sweden. Proceedings of 21st Rock Mechanics Symposium, Rollo, Mo.
- Deer, W.A., R.A. Howie, and J. Zussman, 1962. Rock Forming Minerals. Longmans, Green, and Co., Ltd. London.
- Duane, M.J. and C.T. Williams, 1980. Some Applications of Autoradiographs in Textural Analysis of Uranium-Bearing Samples. Economic Geology, V. 75, pp. 766-770.
- Fritz, P., J.F. Barker, J.E. Gale, 1979. Geochemistry and Isotope Hydrology of Groundwaters in the Stripa Granite: Results and Preliminary Interpretation. Lawrence Berkeley Laboratory report LBL-8285, SAC-12.
- Heinrich, E.W., 1958. Mineralogy and Geology of Radioactive Raw Materials. McGraw-Hill Co., Inc.
- Hood, M., H. Carlsson, and P.H. Nelson, 1979. The Application of Field Data from Heater Experiments Conducted at Stripa, Sweden for Repository Design. Lawrence Berkeley Laboratory report LBL-9392, SAC-26, part II.
- Javandel, I. and P.A. Witherspoon, 1981. Thermal Analysis of the Stripa Heater Test Data. Lawrence Berkeley Laboratory report LBL-13217. In press.
- Nelson, P., B. Paulsson, R. Rachiele, L. Andersson, T. Schrauf, W. Hustrulid, O. Duran, and K.A. Magnussen, 1979. Preliminary Report on Geophysical and Mechanical Borehole Measurements at Stripa. Lawrence Berkeley Laboratory report LBL-8280, SAC-16.
- Schrauf, T., H. Pratt, E. Simonson, W. Hustrulid, P. Nelson, A. Dubois, E. Binnall, and R. Haught, 1979. Instrument Evaluation, Calibration, and Installation for the Heater Experiment at Stripa. Lawrence Berkeley Laboratory report LBL-8313, SAC-25.
- Thorpe, R., D.J. Watkins, W.E. Ralph, R. Hsu, and S. Flexser, 1980. Strength and Permeability Tests on Ultra-Large Stripa Granite Core. Lawrence Berkeley Laboratory report LBL-11203, SAC-31.
- Witherspoon, P.A., N.G.W. Cook, and J.E. Gale, 1980. Progress with Field Investigations at Stripa. Lawrence Berkeley Laboratory report LBL-10559, SAC-27.
- Wollenberg, H., S. Flexser, and L. Andersson, 1980. Petrology and Radiogeology of the Stripa Pluton. Lawrence Berkeley Laboratory report LBL-11654, SAC-36. In press.







This report is part of a cooperative Swedish-American project supported by the U.S. Department of Energy and/or the Swedish Nuclear Fuel Supply Company. Any conclusions or opinions expressed in this report represent solely those of the author(s) and not necessarily those of The Regents of the University of California, the Lawrence Berkeley Laboratory, the Department of Energy, or the Swedish Nuclear Fuel Supply Company.

Reference to a company or product name does not imply approval or recommendation of the product by the University of California or the U.S. Department of Energy to the exclusion of others that may be suitable.

**LBL-14929/SAC-41 Petrologic Changes and Damage in the Stripa Quartz Monzonite**  
**TECHNICAL INFORMATION DEPARTMENT**  
**LAWRENCE BERKELEY LABORATORY**  
**UNIVERSITY OF CALIFORNIA**  
**BERKELEY, CALIFORNIA 94720**